Renewable and Sustainable Energy Reviews 222 (2025) 115990

Contents lists available at ScienceDirect

Renewable and Sustainable Energy Reviews

journal homepage: www.elsevier.com/locate/rser

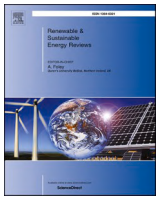

# Floating wind farms in sea basins with moderate wind speeds: a critical assessment of the potential of low-specific-power turbines in reducing the LCoE

Riccardo Travaglini, Francesco Papi *, Alessandro Bianchini

*Department of Industrial Engineering, Università degli Studi di Firenze, Via di Santa Marta 3, 50139, Firenze, Italy*

ARTICLE INFO

*Keywords:*
Floating offshore wind
Low-specific-power turbine
Specific power optimization
Wind farm layout optimization
FOWTs

ABSTRACT

Expanding offshore wind energy in sea basins with moderate wind speeds and higher depths by means of floating offshore wind turbines (FOWTs) is indicated as a priority to meet the challenging goals about renewable energy generation set by many countries worldwide. Upon reviewing the literature, a clear trend emerges for these sites, which suggests prioritizing the development of a different turbine technology with lower specific power than that in use to date, which can be able to ensure suitable energy conversion factors also at lower wind speeds. However, the same review also shows that the potential of low-specific-power rotors has not been studied so far in a sufficiently comprehensive manner to ensure robust assessments. Therefore, the first objective of this study is to develop an original and comprehensive simulation framework for floating wind farms, which is able to account for different rotor designs, floaters, moorings, and farm layouts. The techno-economic data in the model have been synthesized from an extensive and critical review of scientific papers, technical reports, and industry-provided insights. The second objective is then to apply such simulation framework to a variety of sites in the Mediterranean Sea, characterized by different wind speed distributions that span over the range of moderate wind speeds currently under study for new FOWT installations. Results for four rotors, having specific power values ranging from 331 to 175 W/m$^2$, show increases in annual energy production of low-specific-power turbines compared to reference designs that range between 13 % and 30 %, providing potential decreases in LCoE between 3 % and 13 % across the examined locations. Results of this critical perspective are unprecedented in this form and are thought to potentially represent a catalyst for more detailed industrial studies.

## 1. Challenges in floating offshore wind development: a review

The transition to a low-carbon energy system cannot be further delayed if we want to mitigate the impacts of climate change. The European Union, which is at the forefront of this global effort, aims to reach net-zero emissions by 2050 [1]. Offshore wind energy plays a critical role in this shift, as it offers a reliable and scalable renewable energy source, harnessing steadier wind conditions, which can enable higher capacity factors compared to onshore installations [2]. The Global Offshore Wind Report 2024 indicates that Europe remains a leader in offshore wind capacity, with cumulative installations reaching approximately 75 GW by the end of 2023, with a capacity increase of 24 % from the previous year [3]. Currently, the North Sea is the primary region for European offshore wind development, owing to its high average wind speeds (WS) and relatively shallow waters [4]. An estimated 5800 km$^2$ of sea lots will be occupied by offshore farms, corresponding to 170–325 TWh/year, before 2027 [5,6]. These favorable conditions support fixed-bottom turbines, which are well-suited to the region's bathymetry and have been optimized over time to produce power at competitive costs. The report highlights that the Netherlands and the UK are among the largest contributors, with new installed capacity commissioned of 1.9 GW and 833 MW, respectively [7]. Other similar installations can be found in other countries, so far targeting "premium" installation sites with high average wind speeds and shallow waters.

Recent studies have highlighted potential issues in the continued expansion of offshore wind energy in these markets. In fact, the deployment of large-scale wind farms presents multiple challenges, including technical, economic, and environmental issues [8]. For instance, dense clusters of wind turbines may result in revenue reductions due to the wake interactions between aerogenerators. In fact, the more densely packed the turbines, the more relevant the impact of

* Corresponding author.
*E-mail address:* fr.papi@unifi.it (F. Papi).

https://doi.org/10.1016/j.rser.2025.115990
Received 6 March 2025; Received in revised form 19 May 2025; Accepted 21 June 2025
Available online 25 June 2025

**Nomenclature**

*Acronyms*

| | |
|---|---|
| AEP | Annual energy production [GWh/y] |
| asl | Above the sea level [−] |
| CAPEX | Capital expenditure [€/MWh] |
| Cp | Power coefficient [−] |
| Ct | Thrust coefficient [−] |
| FOWTs | Floating offshore wind turbines [−] |
| HVAC | High voltage alternating current [−] |
| HVDC | High voltage direct current [−] |
| LCoE | Levelized cost of energy [€/MWh] |
| LSP | Low specific power [−] |
| MED | Mediterranean Sea [−] |
| OPEX | Operational expenditure [€/MWh/y] |
| POD | Point of delivery [−] |
| RWT | Reference Wind Turbine [−] |
| TI | Turbulence intensity [%] |
| TRL | Technology readiness level [−] |
| TSR | Tip Speed Ratio [−] |
| WS | Wind speed [m/s] |
| WT | Wind Turbine [−] |

*Greek symbols*

| | |
|---|---|
| $\rho$ | air density [kg/m$^3$] |
| φ | torque |

*Latin symbols*

| | |
|---|---|
| *A* | rotor swept area [m$^2$] |
| D | diameter [m] |
| L | height [m] |
| M | mass [kg] |
| R | coefficient of determination [−] |

*Subscripts*

| | |
|---|---|
| BP | bed plate |
| COM | center of mass |
| *DES* | value in design conditions |
| F | floater |
| GEN | generator |
| HUB | hub |
| NAC | nacelle |
| PB | pitch bearing |
| PS | pitch system |
| R | rotor |
| SEC | secondary hub components |
| T | tower |

wakes [9]. The relevance of these losses can be assessed in large offshore wind farms, such as Horns Rev I & Nysted [10,11], where the reported AEP reductions span from 10 to 25 %. Moreover, projections show that for very large-scale wind farms with conventional inter-turbine spacing [12] (e.g., 7 diameters in streamwise and 5 diameters in crosswind directions), AEP losses due to wakes could exceed 60 % [13,14]. In addition, the evermore dense clustering of wind farms in the North Sea has caught the attention of project developers and researchers, which have highlighted potentially significant losses in production due to neighboring wind farm wake effects [15–17]. In addition, clustering offshore wind energy production in a single region can lead to curtailment and grid stability issues, as recently observed in many northern European countries [18–21]. Moreover, even in the absence of curtailment, clustering wind farms in a specific region could also lead to a "self-cannibalization" effect [18], where spot electricity prices are driven down by the high availability of wind energy in periods of high winds in a certain region [22].

Expanding offshore wind energy to other basins, which often have different characteristics from locations that have exploited up to the current point, is seen in all reports as the only way to meet the ambitious targets in terms of offshore wind power generation [23]. In Europe, for example, focus is given to the Mediterranean Sea, as it borders countries with high energy needs that could strongly benefit from local wind energy generation. However, the Mediterranean Sea presents several unique challenges for offshore wind development [24], namely deep waters and a lower average wind resource. Therefore, tailored solutions are required to cost-effectively exploit these regions.

The key component to making offshore wind energy economically viable in deep waters are Floating Offshore Wind Turbines (FOWTs). However, FOWTs are still an emerging technology with high capital and operational costs [25]. Currently, only three floating offshore wind farms, namely Hywind Scotland (30 MW) [26], Kincardine (50 MW) [27], and WindFloat Atlantic (25 MW) [28], are operational and connected to the electrical grid, while several additional projects are in various stages of commissioning, construction, or planning [29]. Despite the rapid advancements in floating wind technology, the levelized cost of energy (LCoE) for floating wind remains substantially higher than that of fixed-bottom offshore wind [29]. The International Renewable Energy Agency recently published a report that anticipates that global offshore wind capacity could reach nearly 1000 GW by 2050. It emphasizes the potential of floating foundations to exploit deeper water resources, projecting that floating wind could account for 5 %–15 % of total offshore capacity by mid-century [30], despite the current high-costs.

### 1.1. Floating farm design: the need for tailored solutions

To increase the competitiveness of floating wind it is necessary to drive LCoE down. From this point of view, according to many experts, FOWTs are a topic with significant margins in terms of technological learning potential [31–33] and significant cost reductions are foreseen within 2030, which could enhance the economic viability of floating wind and enable it to compete with the current costs of fixed-bottom offshore wind [34]. In fact, floating foundation designs have still not coalesced into one, or even a few archetypes. In addition, due to the low-volumes of the floating market, turbines currently used in FOWT applications have been originally designed for bottom-fixed applications and readapted for floating foundations. Recently, the benefits of a more-tightly integrated design of the turbine and floater have been highlighted. Co-design, whereby the controller is designed together with the FOWT system [35], has shown promising results, with measurable reductions il LCoE of up to 4 % that have been found in Ref. [36].

In addition to being able to benefit from a tighter integration with the floating substructures, recent literature has shown the benefits of tailoring the rotor characteristics to the installation site. In fact, Metha et al. [37] have found the optima power to rotor area ratio of offshore wind farms in the North Sea to be close to the industry standard for current offshore turbines, which feature relatively high ratio – i.e., specific power – of 300–350 W/m$^2$. Nevertheless, a measurable benefit in terms of LCoE can be found if scale of the optimum design and specific power are optimized on a site per site basis.

In this context, many researchers have found potential benefits in adapting the turbine diameter through optimization. Serafeim et al. [38] proposed a multidisciplinary optimization to reduce the LCoE of the DTU-10MW Reference Wind Turbine, aiming to estimate the optimum rotor diameter. Results show that the new rotor design, featuring a

larger diameter (+3.7 %) reduced the LCoE by 0.71 % and increased AEP by 2.4 %. Zalkind et al. [39] concentrated on system design for rotors with radii of 100 m or greater, aiming to maximize the AEP while managing overall turbine loads to mitigate increases in operational (OPEX) and capital (CAPEX) expenditures. The framework for blade design examined several design variables, including blade length, cone angle, number of blades, rotor axial induction factor, and the distribution of rotor mass and stiffness to identify the most effective configuration. The authors concluded that an 11 % enhancement in AEP for a 13 MW wind turbine could be realized by extending the blade length by 25 m, corresponding to an increase of 25 %, and reducing the induction factor, all while effectively controlling rotor loads. It must be noted that this approach relies on the optimization of a detailed aeroelastic design of the wind turbine. Therefore, the results in terms of LCoE might be affected by the selected testcase and by the achieved local optimum. In Ref. [40] Buck and Garvey emphasize economic optimization alongside AEP optimization, highlighting that capital expenditures represent the key factor contributing to the total turbine cost in the LCoE equation. They optimized various parameters, including blade chord, axial induction factor, and sectional lift coefficient across the blade span, aiming to minimize CAPEX while enhancing AEP. With reference to the NREL 5 MW offshore turbine, the optimization process achieved a 1 % reduction in CAPEX and a 1.4 % increase in AEP, resulting in an overall improvement of 2.4 % in the CAPEX/AEP ratio.

These analyses, while not all focused on offshore wind farms, suggest that LCoE can be improved by increasing rotor diameter and contextually decreasing specific power. As discussed later on in this study, this trend has indeed been ongoing over the last decade in the onshore market, where a slow but consistent reduction in specific power of new rotors can be observed [22]. In addition, while being able to provide valuable insights on the importance of integrated design on a component level, all these analyses neglect the mutual interactions between the wind turbines within a wind farm. However, changing the rotor diameter influences the wind turbine's wake, in turn influencing inter-array wake losses.

To this end, some authors have included inter-array wake losses in their studies, although often in a simplified manner. Dykes et al. [41] performed a global sensitivity analysis to key wind turbine configuration parameters including rotor diameter, rated power, hub height, and maximum tip speed, by using the integrated wind plant system modeling tool WISDEM. They showed that the increase in turbine diameter might be beneficial to drive LCoE down. Wake losses are estimated as a percentage of the wind farm AEP. Mehta et al. [37] examine how the turbine's rated power and rotor diameter influence various metrics at both the turbine and farm levels, aiming to identify the primary design drivers and understand how they affect different configurations. They developed an optimization framework able to minimize the LCoE and define the optimal turbine size. They found that reconfiguring the IEA 15 MW turbine for an installation site in the Dutch North Sea results in an optimal wind turbine with a rated power of 16 MW (+6.7 %) and a diameter of 236m (−1.5 %), leading to a LCoE improvement of approximately 1 %–2 %. The increase in turbine-specific power with respect to the reference is motivated by the high wind speeds of the studied sea basin. Wake losses are once more considered approximately, as the wind farm layout is not a design variable and is considered fixed in the study.

Both studies are based on complex multi-disciplinary design frameworks. Other authors have tackled the problem from a different perspective, using much simpler models based on empirical cost-scaling rules. Shields et al. [42] studied the impact of turbine upscaling and plant upsizing on various farm-level parameters. They found a reduction in LCoE by up to 20 % when upscaling turbines from 6 to 20 MW and upsizing the farm from 500 MW to 2500 MW capacity. However, the study assumes a fixed cost per kW for the turbines and also limits the specific power of the turbines when upscaling. Ashuri et al. [43] optimized a 5 MW reference turbine and scaled it up to 10 and 20 MW, respectively, to evaluate the effect of rotor and tower upscaling on LCoE. Their study claims an increasing LCoE trend when upscaling. However, the costs for balance of system (BoS) and O&M are assumed to scale with the rated power, with a fixed value for the exponent, following the relations presented in Ref. [44], thus strongly simplifying the complex relationships of the turbine with other elements of the farm. Sieros et al. [45] performed an upscaling study for turbines in the range of 5–20 MW, with constant specific power, using classical similarity rules. The results showed an increase in the levelized production cost with turbine scale, for the same technology level. However, the focus of the study was on a simplified upscaling method, especially for the turbine, while the models for the rest of the wind farm were expressed simply as a percentage of turbine costs.

Finally, some researchers have shown that it is possible to focus on metrics other than LCoE as wind farm design drivers. The research conducted by Canet et al. [46], despite focusing on on-shore wind, shifts the focus from solely power generation and economic factors to long-term sustainability and lifetime CO2 emissions. This study established a relationship for $CO_2$ emissions that parallels the LCoE equation, defined as the environmental value minus the environmental cost divided by the total energy produced. Utilizing this new metric, the researchers optimized hub height and rotor diameter ($D_R$) to reduce environmental impact. Their findings indicated that the optimal configuration for environmental considerations does not align with the LCoE optimal configuration. More interestingly, they show for a test case in Germany that Low Specific Power (LSP) aerogenerators can be beneficial for both the cost of energy and the environmental impact due to the increased production at low wind speeds. Nevertheless, these results may not directly translate to offshore installations. In fact, inland installations do not require an upscaling of the offshore foundation or floating platform, which strongly affects the CAPEX of the system. Additionally, the wind farm layout is often constrained by terrain morphology, and thus it often does not represent a design variable for the system. If this is the case, the stronger wake effects due to the enhanced swept areas cannot always be offset by an increase in spacing between wind turbines, contrary to what may be possible offshore. These latter works put more emphasis on economic assessments, often prioritizing cost-related metrics over physical accuracy. While valuable for early-stage evaluations, such simplifications limit the ability to derive insights into the complex dynamic interactions that govern system behaviour. In addition, the cost-scaling rules employed in these studies often neglect the influence of swept area, and are based or nameplate power output, and are thus not suitable for studying the influence of rotor FOWT design on LCoE.

Another class of studies focuses on wind farm layout. In fact, considering wind farm layout in the design process allows for design techno-socio-economic tradeoffs between often conflicting interests such as the minimization of wake losses, the minimization of inter-array cable costs, the reduction of visual impact and the reduction of sea use, often contested with other activities such as tourism or fishing, to be evaluated. Furthermore, rotor diameter influences FOWT spacing significantly, as it impacts wake losses and thus energy production and structural loading. At the same time, FOWT spacing impacts the inter-array (IA) cable length, the cost of which per unit length is significant [47]. Moreover, considering the wind farm layout in the design process allows for additional design variables to be considered, such as the mooring lines, which can decrease inter-array wake losses significantly [48]. Many researchers have tackled this issue by developing and utilizing wind farm layout optimization tools. Yilmazlar et al. [49] presented a modular tool for preliminary estimation of the LCoE in wind farms, supporting early-stage design decisions through simplified models. While the tool effectively captures interactions between layout and cost components, such as the trade-off between reduced wake losses and increased cabling costs with larger turbine spacing, it does not perform any wind turbine design. Moreover, the case study is limited to a parametric analysis of inter-turbine spacing using FLORIS [50],

varying only the distances between turbines without changing their orientation. Such parametric approaches may overlook more optimal solutions, as they fail to explore the full design space or account for the coupled effects of layout and turbine characteristics.The research conducted by Hietanen et al. [51] concentrated on optimizing the layout of offshore wind farms, aiming to decrease the LCoE for floating offshore wind installations by integrating floating-specific parameters with economic indicators. Their optimization routine identifies rotor placement across various offshore wind farms using an objective function that seeks to maximize AEP while adhering to constraints related to CAPEX and OPEX. While this optimization encompasses multiple parameters, its primary focus is not on the design of the wind turbines themselves but rather on the installation of rotors and the associated transmission requirements, which constitute significant costs for floating offshore wind farms. Cazzaro and Pisinger [52] addressed the scalability limitations of traditional methods by proposing a variable neighborhood search-based heuristic capable of efficiently optimizing layouts for large-scale offshore wind farms. Their method incorporates realistic constraints such as turbine spacing and foundation costs and demonstrates high performance even on problem instances involving thousands of potential turbine locations. Cao et al. [53] contributed a multi-objective optimization framework that considers not only power generation but also the distribution of streamwise turbulence intensity, a critical factor influencing turbine fatigue life. By integrating a turbulence-aware wake model and employing a genetic algorithm, their approach successfully reduces operational stress on turbines while maintaining energy production levels. Thomas et al. [54] presented a comprehensive comparative analysis of eight optimization methods applied to a standardized layout optimization case study, highlighting the importance of algorithmic transparency and reproducibility. Their results revealed that diverse methods can yield comparable performance when applied correctly, emphasizing the robustness of current optimization techniques. Lei et al. [55] proposed an adaptive genetic-particle swarm hybrid algorithm that dynamically modifies turbine positions to enhance conversion efficiency across varying wind scenarios and constraint sets. This approach achieved superior performance compared to a range of benchmark algorithms, underscoring the potential of hybrid metaheuristics. Finally, Yang et al. [56] advanced the field by shifting the optimization objective from power maximization to minimization of the LCoE, using an improved analytical wake model combined with a hybrid optimization strategy. Their method demonstrated notable gains in energy efficiency and cost-effectiveness, particularly in large-scale deployments. Collectively, these studies reflect the significant progress made in the development of increasingly sophisticated algorithms for optimizing wind farm layouts under realistic environmental and operational constraints. However, a common limitation across this body of work is the assumption of fixed turbine characteristics, regardless of the specific wind resource at a given site. By treating turbines as standardized components rather than as design variables that can be adapted to local wind conditions, these approaches may overlook substantial opportunities for improving overall wind farm performance.

In addition to the aforementioned classes of studies, some researchers have also focused on evaluating the impact of floating wind farms more broadly from an energy-system perspective. Martínez and Iglesias [57] evaluated LCoE across the Mediterranean using static wind resource data and basic power curve models, overlooking the dynamic effects of floating structures and atmospheric variability. Ghigo et al. [58] focused on minimizing platform weight to reduce costs, but their analysis did not capture the coupled dynamics of platform motion and turbine performance. Lerch et al. [59] performed a broad sensitivity analysis on LCoE for various floating wind farms concepts, yet their methodology was grounded in parameterized cost inputs and deterministic energy estimates. Similarly, Lanni et al. [60] explored floating wind farms for hydrogen production using a streamlined economic model that neglected the complex physical behaviour of floating systems in real sea conditions. While all these studies offer valuable insights into cost structures and deployment strategies, their reliance on simplified simulations limits their ability to represent the intricate physics of floating wind farms. Accurate assessment of energy production, structural loading, and long-term performance in floating systems requires integrated, high-fidelity models that couple aerodynamic, hydrodynamic, and control system interactions—elements that remain largely unaddressed in this research branch.

Overall, these analyses show that tailoring the wind turbine to the specific installation location by changing design parameters such as rated power, nominal rotor loading and blade length can benefit LCoE. At the same time, optimizing the wind farm layout, despite being an algorithmically complex problem due to the large number of design variables involved, can also benefit LCoE. While this literature review has also highlighted the existence of broader system-level studies focused on the impact of FOWTs in sea basins such as the Mediterranean, no study was found to date where the influence of design parameters on the wind farm layout has been studied. This gap highlights the need for an integrated optimization framework that considers both the spatial configuration of wind farms and the design of turbines, tailored to the unique wind profiles of each location.

### 1.2. Objectives and structure of the study

Based on the presented context, the objective of this paper is to investigate the potential of LSP rotors in moderate wind speed offshore basins. To accomplish this objective a framework that is able to account for the influence of the wind farm layout and design parameters simultaneously in a physically consistent manner is developed. Furthermore, a detailed review of existing cost and mass scaling function for various turbine components is provided throughout the manuscript. A decrease in specific power is indeed a trend that has been ongoing for several years in onshore wind installations [22,61]: this trend has provided increased capacity factors for onshore wind projects despite them being developed in lower wind speed sites [62], and has led to the development of LSP rotor designs in academia [22]. In addition, despite the potential benefits of LSP rotors that have been discussed in the literature review in the previous section, this is a topic that is yet to be extensively explored for FOWTs. More specifically, both commercial and reference turbines developed by the academic community to date [63,64] are designed and optimized for those high wind speed conditions usually targeted by bottom-fixed applications [37]. As discussed, however, many offshore basins with significant development potential such as the Mediterranean Sea experience significantly lower average wind speeds (WSs) compared with northern European waters [4,65]. The overall energy conversion potential of commercial turbines in these sites is thus reduced. To this end, researchers are investigating (e.g., the EU project FLOATFARM [66]) the possibility of creating a new generation of FOWTs tailored to moderate wind speed deep-water sites and characterized by a lower specific power, i.e., the ratio between generator power and rotor swept area. From a technical perspective, lower specific power can be achieved by maintaining the same generator power and upscaling the rotor or by decreasing the generator power for a given rotor. In the context of FOWTs, however, both strategies involve some drawbacks. The first approach leads to taller and heavier towers, which in turn result in a significantly increased overturning moment on the floating substructure, which needs to be increased in size, using more material and increasing cost. On the other hand, in the second strategy, it is apparent that the turbine and the substructure, designed to cope with higher aerodynamic loads, are underexploited and are therefore not cost-effective.

The present study aims to critically discuss the prospects of using LSP wind turbines in floating offshore installations in sites with moderate wind speeds. The workflow of the study is presented in Fig. 1. First, the literature review presented in the previous sections allowed for the definition of a broader framework of the problem. In particular, it is apparent that, contrary to the few studies presented to date (e.g.,

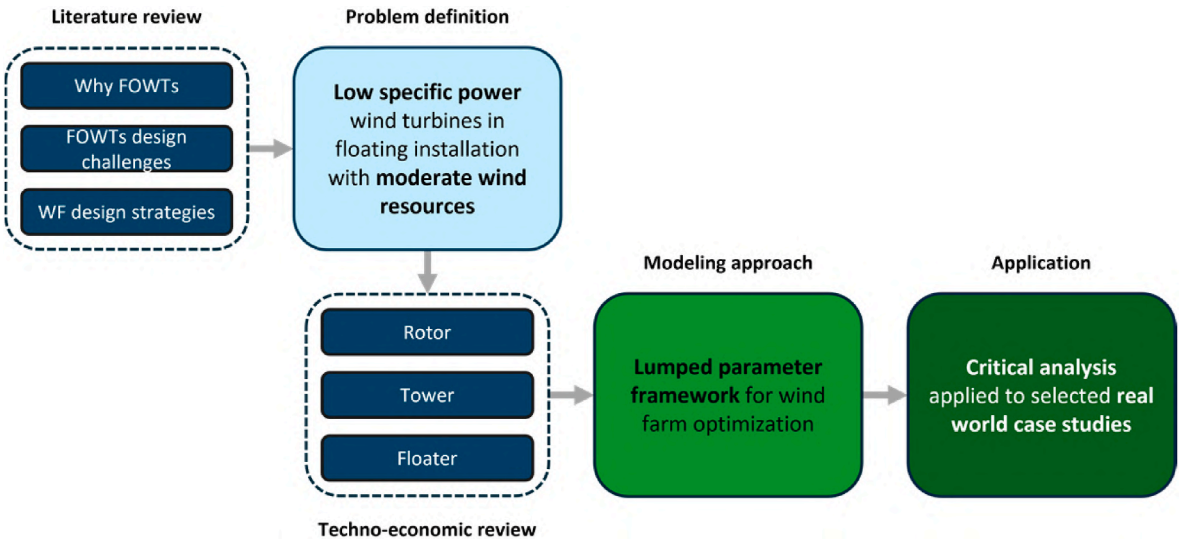


**Fig. 1.** Workflow of the study. Review phases are highlighted with dashed boxes.

Ref. [67]), estimating FOWT prospects in new sea basins with simplified analyses that only estimate the aerodynamic AEP as a combination of statistic wind profiles (i.e., the wind distribution in the sites) and hypothetical power curves for this new rotors may result in unrealistic estimations. On the other hand, a comprehensive approach is needed, which must be able to evaluate the tradeoffs in terms of wake effects, cable costs, substructure, and turbine on CAPEX, OPEX, and energy production: a simple reanalysis of existing data cannot be sufficient for the scope.

Based on these outcomes, detailed reviews have been carried out on existing modeling tools and techniques for the main components of FOWT farms. For each of these components, namely the rotor, the tower, and the floater, an extensive literature review, focused on how these component's mass and cost scale with FOWT size is first provided, followed by a discussion on how realistic scaling models for each of them can be derived and included a comprehensive simulation framework. This framework represented the key enabler to investigate how reduced-specific-power turbines can be effectively integrated into floating wind farms to enhance the economic viability of floating offshore wind projects in moderate wind speed conditions. Although both the models and the conclusions are of general interest for all other installations with similar bathymetry, such as the Atlantic shores of the United States of America or waters around Japan, for the purposes of the present study, the Mediterranean Sea is taken as the case study to investigate critically the potential of LSP FOWTs due to its unique wind resource. By selecting the Mediterranean Sea as a case study, we had access to different sites that are representative of a quite broad spectrum of moderate wind conditions, thus allowing one to assess the complex interactions between turbine design variables and farm-level economics, offering insights into the prospects of the technology.

The study is structured as follows. The selected study cases are presented in Section 2. The review studies for each of the main system components and their implementation into a unique framework are reported in Section 3. Section 4 presents the optimization algorithm, while Section 5 discusses the results of the analyses on the Mediterranean case studies. These are followed by a critical discussion on the prospects of technology (Section 6). Final remarks, best practices, and possible further developments are finally outlined in Section 7.

## 2. Study cases

As discussed in Section 1, evaluating the techno-economic potential of LSP floating rotors requires going into the details of the selected study cases, as no high-level analysis based on aggregate data or average value has the potential to provide accurate insights.

### 2.1. Turbines

The present study considers four 15-MW wind turbines, purposefully designed for this analysis. Diameters range from 240 m, which corresponds to the current academia-designed reference 15 MW wind turbine by IEA [63], to 330 m, in a 30 m step. Specific power ranges from 331.6 to 175.4 W/m$^{2,}$ respectively. Table 1 highlights the most significant parameters of the proposed WTs. Hub height is estimated by adding 30 m to the rotor radius in order to ensure sufficient sea clearance. Although the literature lacks clear guidelines on how to calculate minimum sea level clearance of the blades, the authors decided to operate in similitude with the most recently developed FOWTs, namely the IEA 15 and 22 MW RWT [63,64], where the same length has been set as the minimum tip clearance from the sea. The turbines are installed on semi-submersible platforms with a 20 m freeboard height. The naming scheme of the turbines, shown in Table 1, reflects the area of interest for the turbines (MED – Mediterranean Sea), the rated power of the machines, and their diameter.

### 2.2. Farm layout

The four turbine designs are used to estimate the overall performance of wind parks in various strategic locations in the Mediterranean. Each farm is supposed to have a total installed capacity of 1.005 GW, i.e., obtained by the deployment of 67 FOWTs. Regarding the electrical infrastructure, one central substation has been included to accommodate the electricity infrastructure needed for the voltage increase needed to deliver electricity through the high-voltage alternating current export cables (HVAC). The electricity is transmitted to the point of delivery (POD) onshore using the HVAC technology, considering the reduced costs, with respect to the direct current cables [68], related to an export distance that does not exceed 60 km. In order to simplify the infrastructure needs, any onshore electrical system has been neglected, assuming the POD is located in close proximity to the shores. Notably, the design does not incorporate an energy storage system, assuming a direct integration with the grid and focusing only on the production system. As better described in Section 4.4, for each installation site, the available area for the wind farm is assumed to be squared, with a surface area of 450 km$^2$. The available sea lot has been assumed oriented with its upper side parallel to the east-west direction for all the test cases.

**Table 1**
Main design parameters for the IEA15MW RWT and the proposed FOWTs.

| Wind Turbine | RWT [63] | MED15MW_240 | MED15MW_270 | MED15MW_300 | MED15MW_330 |
|---|---|---|---|---|---|
| **Hub height [m]** | 150 | 150 | 165 | 180 | 195 |
| **Tower Height ($H_T$) [m]** | 130 | 130 | 145 | 160 | 175 |
| **$D_R$ [m]** | 240 | 240 | 270 | 300 | 330 |
| **Specific power [W/m$^2$]** | 331.6 | 331.6 | 262.0 | 212.2 | 175.4 |
| **Rated power [MW]** | 15 | 15 | 15 | 15 | 15 |
| **Cut in/out WS [m/s]** | 3/25 | 3/25 | 2.8/25 | 2.6/25 | 2.5/25 |
| **Rated WS [m/s]** | 10.7 | 11.3 | 10.5 | 9.9 | 9.5 |

### 2.3. Wind dataset

Wind speed data is sourced from the ERA5 reanalysis database [69]. A time span of thirty years has been selected, from 1993 to 2023. ERA5 provides the wind source data at a maximum height of 100 m above sea level (a.s.l.). To account for the height difference between the ERA5 data source (100 m) and the turbine hub heights, which range between 130 and 175 m, a power-law shear factor was employed to extrapolate wind speeds. A shear exponent of 0.1 has been selected relying on the findings of Yan et al. [70] for regional offshore conditions, ensuring consistency with expected atmospheric dynamics over the sea.

### 2.4. Installation sites

The installation sites selected for this work have been chosen to represent several wind resource conditions across the Mediterranean Sea. As shown in Fig. 2a, this water basin experiences a high variability of the wind resource. Additionally, even in the most promising sites such as the Gulf of Lyon, there is a significant difference in energy content with respect to the class I reference Weibull [71]. While the latter experiences an energy density of 340.5 kWh/m$^2$, the installation site in France is characterized by an energy content of 182.4 kWh/m$^2$, much closer to the 167.3 kWh/m$^2$ of the class III reference source. This is also consistent with the average wind speed experienced by the installation sites. These values range between 5.6 m/s and 7.6 m/s, highlighting moderate wind regimes closer to the 7.5 m/s of the Class III than to the 10 m/s of the Class I [71]. Fig. 2a also shows a comparison between the Class I wind source and the Weibull in an installation site in the Dutch North Sea (Nederwiek) [72], which provides a wind resource similar to the one of the reference class, corroborating the hypothesis that existing offshore wind turbines have been tailored to this sea region. As shown by the contour map in Fig. 2b [73], the chosen sites in the Mediterranean range from Cyprus, characterized by the lowest average wind energy, to Lyon, which experiences the most favorable wind conditions. Overall, a significant range of "moderate" wind scenarios is considered, allowing for a robust assessment of the LSP turbine technology. Table 2 summarizes the main characteristics of selected installation sites; more info can be found in Appendix A.

## 3. FOWT cost and scaling models: review and critical assessment

Despite the presence of some cost and mass scaling laws in the open literature, WT upscaling in unconventional offshore environments represents a gap in existing research. While few approaches have been proposed in previous studies, they consider the upscaling of both rotor swept area and installed power [77], and do not match the purpose of this analysis. Other validated cost and mass scaling models proposed in the literature [44,78] focus instead on onshore or fixed-bottom WTs. On the other hand, as shown in section 1.3, many of the existing studies propose approaches in which the full aeroelastic design of a wind turbine is performed. In the next sections, a novel, simpler approach is proposed based on a synthesis of the most credited data available both in the relevant academic literature and in industry reports. This system-level method entails the adoption of scaling laws for the replacement of the complex algorithms and procedures needed for the structural and aerodynamic design of aerogenerators. Therefore, it allows for easy preliminary analyses on the feasibility of a WT with a fixed specific power in an installation site characterized by a known Weibull curve, while remaining physically consistent. As discussed, this complex assessment is key if one wants to get a sufficiently reliable overview of the problem, since all the studies presented to date fail in capturing the complex implications of upscaling FOWTs.

### 3.1. Rotor performance

In order to isolate the effect of specific power variation on LCoE and avoid the results being affected by a specific aerodynamic design, the IEA 15 MW FOWT [63] is taken as a reference. The scaled rotors defined in this study are assumed to be aerodynamically similar and have the same performance maps in terms of power, thrust, and torque coefficients of the reference rotor [79]. While representing a simplification, this assumption is thought to be quite realistic, as the aerodynamic efficiency of the reference rotor is still at the edge of current standards. The power output of a wind turbine can be expressed as a function of the wind speed, its efficiency, and the rotor area as in Eq. (1):

$$P = \frac{1}{2} * \rho * A * Cp(\lambda, \beta) * WS^3 \tag{1}$$

where $\rho$ represents the air density, $A$ the WT swept area, and $Cp$ the power coefficient as a function of the main turbine operating parameters, tip-speed ratio, and blade pitch angle. As Eq. (1) indicates, in the assumption that the same power coefficient can be maintained, the power output scales favorably as the swept area increases. If power in Eq. (1) is fixed to the design, or rated, power output, the rated wind speed ($WS_{DES}$) (Eq. (2)) at which such power is produced decreases as the swept area increases:

$$WS_{DES} = \sqrt[3]{\frac{P_{DES} * 2}{A * Cp * \rho}} \tag{2}$$

Therefore, an increase in specific power in the form of an increase in rotor diameter while maintaining generator power constant results in a shift to the left of the wind turbine power curve.

Similarly to power output, thrust ($T$), the total axial aerodynamic force of the rotor, can also be expressed as a function of swept area and wind speed as in Eq. (3):

$$T = \frac{1}{2} * \rho * A * Ct(\lambda, \beta) * WS^2 \tag{3}$$

where $Ct$ is the thrust coefficient of the rotor. Both these high-level parameters are important as power directly influences turbine output and plant revenue and thrust is directly correlated to aerodynamic loading on the structure and also influences wake strength and development. Both parameters, however, cannot be estimated directly but rather depend on the operational parameters $\lambda$ (tip-speed ratio – TSR) and $\beta$ (blade pitch angle), which in turn depend on the specific rotor aerodynamic design. Assuming similarity to the IEA 15 MW FOWT, the operational strategy can be determined. If the rotor speed is between the minimum ($\omega_{min}$) and maximum ($\omega_{min}$) the rotor operates at the IEA 15 MW design TSR of 9, where optimal performance is reached. The TSR is

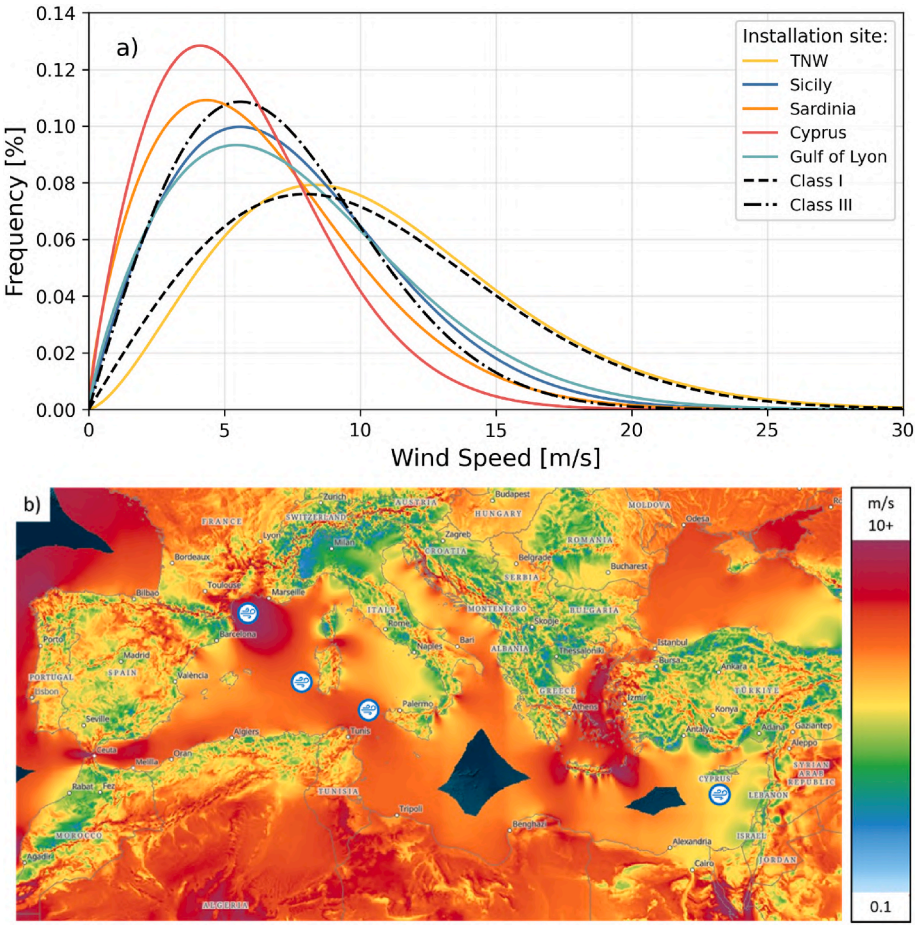


**Fig. 2.** Comparison between the Weibull (a) of the considered installation sites (b) at 100 m asl. Wind speed map from Global Wind Atlas[1].[1]

**Table 2**
Installation sites comparison.

| Wind Turbine | Lyon | Sicily | Sardinia | Cyprus |
|---|---|---|---|---|
| **Average WS [m/s]** | 7.6 | 7.4 | 6.4 | 5.94 |
| **Weibull shape factor (k) [−]** | 1.79 | 1.89 | 1.72 | 1.89 |
| **Export distance [km]** | 20 | 60 | 35 | 25 |
| **Average sea depth [m]** | 85 | 390 | 300 | 350 |
| **Prevalent wind direction [−]** | W-N-W | N-N-W | W-N-W | W |
| **Source [−]** | [74] | [75] | [76] | |

defined in Eq. (4):

$$\lambda = \frac{\omega R}{WS} \tag{4}$$

The minimum and maximum rotor speeds can be derived in analogy to the IEA 15 MW by imposing that the scaled rotors operate at the same TSR as the reference turbine at cut-in (Eq. (5)):

$$\lambda = \frac{\omega_{IEA15}^{cut-in} R_{IEA15}}{WS_{IEA15}^{cut-in}} = \frac{\omega_i^{cut-in} R_i}{WS_i^{cut-in}} \tag{5}$$

Which leads to:

$$\omega_i^{cut-in} = \frac{R_{IEA15}}{R_i} * \frac{WS_i^{cut-in}}{WS_{IEA15}^{cut-in}} * \omega_{IEA15}^{cut-in} \tag{6}$$

Eq. (6) relates the cut-in rotor speed to the radius of the reference and scaled machines, to the cut-in rotational speed of the reference machine and to the cut-in wind speed of the reference and scaled turbine. The latter parameter, however, is unknown. This limitation can be overcome by imposing that the scaled turbines must produce the same power as the reference IEA 15 MW machine at cut-in (Eq. (7)):

$$P_{cut-in} = \frac{1}{2}\rho\pi R_{IEA15}^2 C_p WS_{IEA15}^{cut-in\,3} = \frac{1}{2}\rho\pi R_i^2 C_p WS_i^{cut-in\,3} \tag{7}$$

Eq. (7) can be inverted and simplified to obtain Eq. (8):

$$\frac{WS_i^{cut-in}}{WS_{IEA15}^{cut-in}} = \left(\frac{R_{IEA15}}{R_i}\right)^{2/3} \tag{8}$$

which allows the cut-in wind speed of the scaled rotors to be determined. Finally, if this expression is substituted into Eq. (6), the cut-in minimum rotor speed (Eq. (9)) is determined:

$$\omega_i^{cut-in} = \left(\frac{R_{IEA15}}{R_i}\right)^{5/3} * \omega_{IEA15}^{cut-in} \tag{9}$$

The same procedure is then repeated at the rated wind speed, where all designs must output 15 MW of power, to determine the nominal rotor speed and rated wind speed. If the rotational speed required to maintain the optimal TSR of $\omega = \lambda WS/R$ is lower than the minimum rotational speed as determined in Eq. (9), the rotor operates at the minimum rotational speed.

A power-maximizing pitch angle is numerically selected for the resulting TSR from the *Cp* map, ultimately resulting in the non-zero pitch angle shown in Fig. 1b when the TSR (shown in Fig. 3a) exceeds the IEA 15 MW-nominal value of 9. As shown in Fig. 3, four different aerodynamically-similar rotors have been evaluated in this study, with diameters, ranging from 240 to 330 m, in a 30 m step, corresponding to a specific power that ranges from 331.6 to 175.4 W/m$^2$ respectively. Once the operational point is set, rotor power and thrust can be determined from the *Cp* and *Ct* maps, respectively. The obtained values of power and

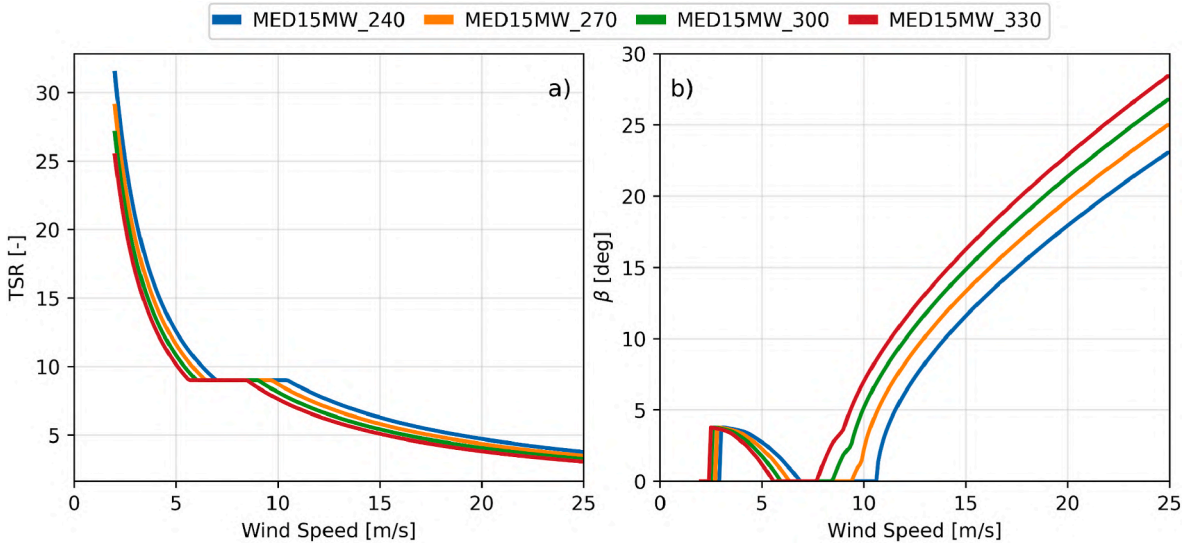


**Fig. 3.** WT power curves in the laminar (a) and turbulent (b) free stream wind conditions.

thrust are shown in Figs. 3 and 4.

In order to limit the aerodynamic loads on the upscaled rotors, peak shaving, whereby the blades of the turbine are feathered before rated power is reached in order to shave load, is also implemented. As better explained later in the study, the use of peak shaving is a common load-reduction technique and is especially significant in load-constrained LSP rotors. As shown in Ref. [64], this technique allows for significant peak load reduction with often minimal AEP losses. The effect of this strategy is highlighted in the rotor thrust curves in Fig. 4. In addition, the increase in blade pitch required to limit rotor thrust can be seen in Fig. 3b, where all curves except the one relative to the MED15MW_240 FOWT, which does not employ peak shaving, feature a more gradual "knee" before the rated wind speed. From a model perspective, if rotor thrust exceeds a user-specified threshold, the pitch angle that is able to satisfy the imposed constraint is determined numerically from the *Ct* response curve. Finally, the newly determined combination of TSR and pitch angle is then used to determine rotor power.

In the final step, rotor power is corrected for the effect of turbulence intensity using the empirical model of Saint-Drenan et al. [80], using the average turbulence intensity from the FINO1 [81] offshore installation site as representative of the turbulence intensity in a generic offshore site. The effect of turbulence intensity (TI) on the rotor power curve is shown in Fig. 5. This effect has been neglected in almost all the techno-economic feasibility studies presented to date on the topic, but it is thought to have a non-negligible effect on the final results, especially around rated wind speeds.

### 3.2. Component mass and cost

Changing rotor-swept areas leads not only to a different performance of the turbine, but also to different loads. In turn, changing the loads means that the structural properties and cost of the turbine change. In order to account for the effect of such load changes, without performing a complete re-design of the machine, the authors prioritized a simplified correlation-based approach.

[1] Map obtained from the Global Wind Atlas version 3.3, a free, web-based application developed, owned and operated by the Technical University of Denmark (DTU). The Global Wind Atlas version 3.3 is released in partnership with the World Bank Group, utilizing data provided by Vortex, using funding provided by the Energy Sector Management Assistance Program (ESMAP). For additional information: https://globalwindatlas.info.

#### 3.2.1. Tower

The NREL cost and scaling model [44] is used as a basis to determine the mass and, consequently, the cost of the FOWT towers. In analogy to this model, the mass of the tower ($M_T$) as a function of its height ($L_T$) is determined according to a power law $M_T = \alpha L_T^{\beta}$. Floating towers are generally designed to be stiff-stiff, with natural frequencies placed above the 3P excitation range. As such, mass scaling correlations determined for onshore towers are inaccurate if applied to FOWTs. Therefore, in order to calibrate the law an extensive literature review has been performed. However, due to the deployment of only a few demonstrators, only the seven sources listed in Table 3 have been included. Starting from the existing literature, a correlation has been developed relying on the relationship between $M_T$ and $L_T$. The trendline resulting from the fitting reported in Eq. (3) (Eq. (10)) has been adopted to obtain the $M_T$ of the new WTs relying only on their $L_T$.

$$M_T = 1479.457 * L_T^{1.396} \tag{10}$$

Fig. 6 and Table 3 show the results of the fitting for the MED FOWTS (orange points). The outcomes obtained show a good agreement with the literature data, highlighted by the trendline coefficient of determination ($R^2$) equal to 0.8.

#### 3.2.2. Rotor nacelle assembly

An approach similar to the one adopted for the tower has also been adopted for the RNA. For the RNA, the authors opted for the DTU mass scaling model, due to its development specifically tailored for offshore wind farms [78]. However, as shown in Table 4, to estimate the effect of the increased $D_R$ on blade masses, the correlation developed by NREL [44] has been utilized. This model, in fact, allows for the choice of the turbine class, which leads to a more accurate fit for the specific requirements of the analyzed test case. Specifically, rotor mass ($M_R$) has been calculated with Eq. (4) in Table 4, where the exponent is related to class III turbines with carbon fiber spar caps. No additional FOWT-specific calibration was performed as blades are amongst the least affected components, loads-wise, when a turbine is installed on a floating foundation [86,87].

In order to univocally define the center of mass of the turbine ($H_{COM}$), the mass of the nacelle ($M_{NAC}$) needs to be accounted for. This parameter accounts for the weight of the nacelle housing per se, which is supposed to be independent of rotor size and the internal components. The dependency on $D_R$ for the parts mentioned above is modelled with the DTU mass scaling model as shown in Table 4. Specifically, the masses of rotor, hub ($M_{HUB}$), pitch bearings ($M_{PB}$), pitch system ($M_{PS}$), and drivetrain

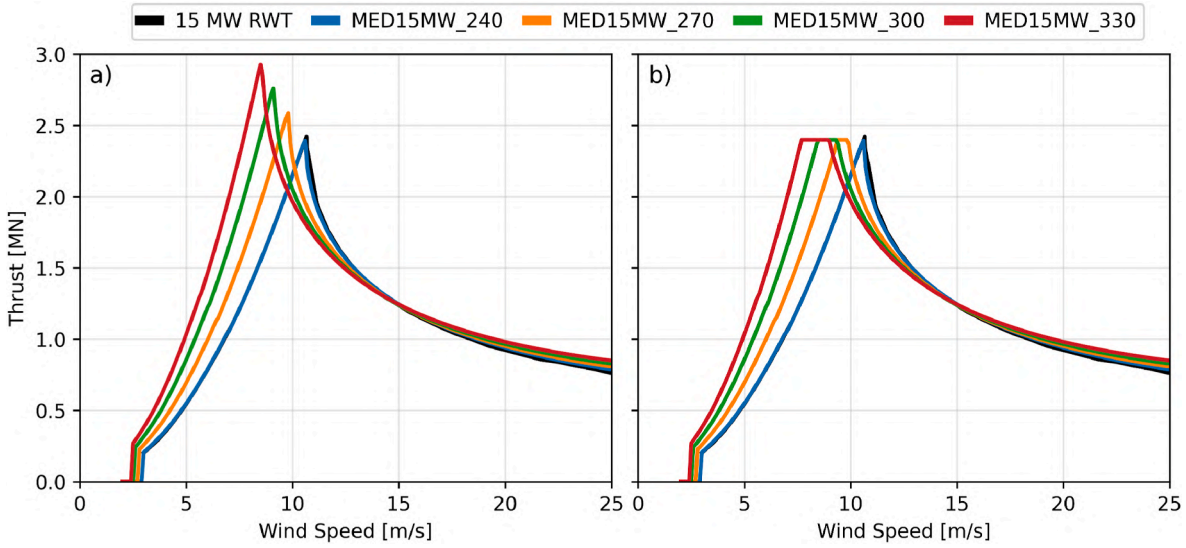


**Fig. 4.** WT thrust curves without (a) and with (b) active pitch control.

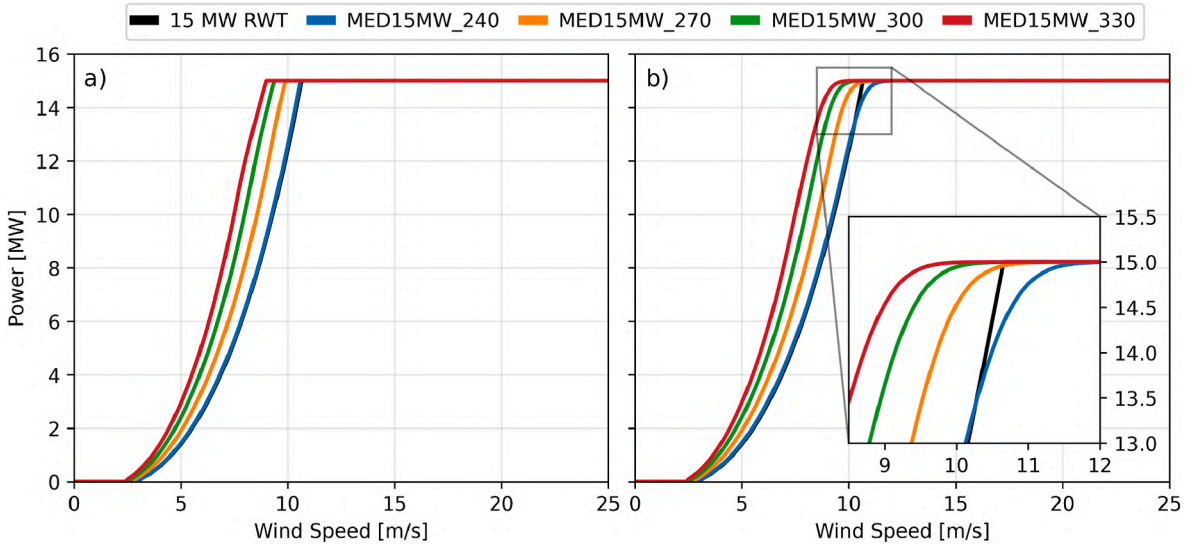


**Fig. 5.** WT power curves in the laminar (a) and turbulent (b) free stream wind conditions.

**Table 3**
Existing and proposed FOWTs' $M_T$ and $H_T$.

| Wind Turbine | P [MW] | $H_T$ [m] | $M_T$ [t] | Source [−] |
|---|---|---|---|---|
| Hywind | 6.0 | 83.0 | 670.0 | [26] |
| 10 NAUTILUS | 10.0 | 107.0 | 879.0 | [82] |
| 10 MW OO-STAR | 10.0 | 104.6 | 1257.0 | [82] |
| 15 MW Volturn US-S | 15.0 | 130.0 | 1259.0 | [77] |
| 15 MW Corewind | 15.0 | 120.5 | 1088.5 | [83] |
| IEA-15-240-RWT | 15.0 | 130.0 | 1478.6 | [84] |
| IEA-22-280-RWT | 22.0 | 150.0 | 1574.0 | [85] |
| MED15MW_240 | 15.0 | 130 | 1324.4 | – |
| MED15MW_270 | 15.0 | 145 | 1542.6 | – |
| MED15MW_300 | 15.0 | 160 | 1769.9 | – |
| MED15MW_330 | 15.0 | 175 | 2005.8 | – |

bedplate ($M_{BP}$) are strongly affected by $D_R$, and an increased rotor swept area leads to increased masses and loads. Regarding the generator ($M_{GEN}$), equation (10) shows a dependency on rated torque ($\varphi_{DES}$), which is again directly related to the $D_R$.

Finally, mass correlations for minor components, such as the nacelle and drivetrain bedplate, can be found in the documentation of the model [78] and are not herein reported.

To estimate the cost of each of the RNA's components, the cost scaling model developed by DTU has been utilized [78]. Costs are estimated as a function of the component masses. Specifically, Eq. (16) shows the linear relation between the cost of the specific component ($C_i$) and its mass, where $\beta$ represents the cost scaling factor.

$$C_i = \beta^* M_i \tag{16}$$

Eq. (11) is applied to all RNA components, as well as to the tower and blades. The specific value of $\beta$ is reported in Ref. [78] for each component.

The resulting mass of the WTs is reported in Table 5, with a focus on the $H_{COM}$. This parameter has been calculated as in Eq. (17), by assuming the RNA $H_{COM}$ at the hub height, and the tower $H_{COM}$ at 40 % of the $H_T$. This assumption is consistent with the data reported in Refs. [84,85], where the average tower center of mass is located at about 40 % of the tower height.

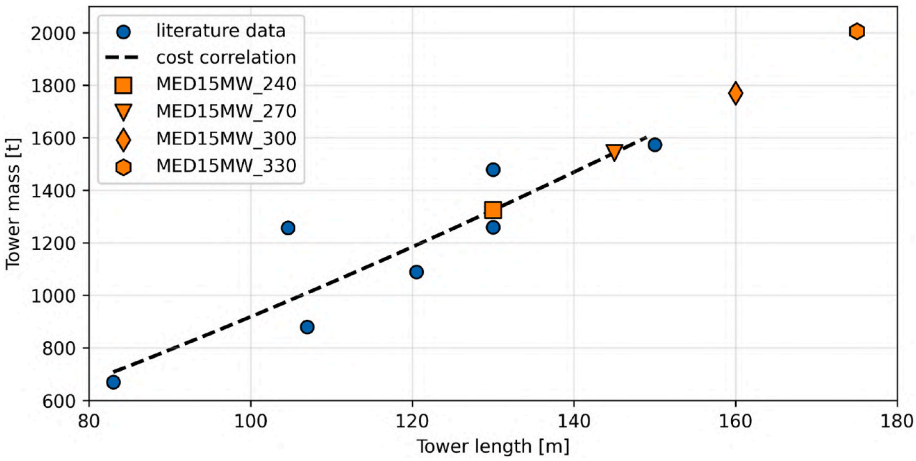


**Fig. 6.** $M_T$ literature and proposed data relying on the introduced correlation.

**Table 4**
Mass scaling equations for the main RNA components.

| Component | Mass Equation | Equation number | Source |
|---|---|---|---|
| Rotor | $M_R = 3*0.5*(0.5*D_R)^{2.44}$ | (11) | [44] |
| Hub | $M_{HUB} = 6*10^3 + 0.1*D_R^{2.5}$ | (12) | [78] |
| Pitch bearings | $M_{PB} = 5*10^2 + 0.07*D_R^{2.5}$ | (13) | [78] |
| Pitch system | $M_{PS} = 5*10^2 + 0.03*D_R^{2.5}$ | (14) | [78] |
| Drivetrain generator | $M_{GRN} = 35*10^3*\varphi_{DES}^{0.7}$ | (15) | [78] |

**Table 5**
Proposed FOWTs' $M_R$, $M_{TOT}$ and $H_{COM}$.

| Wind Turbine | $D_R$ [m] | $M_R$ [t] | $M_{TOT}$ [t] | $H_{COM}$ [m] | $OM_{STD}$ [MNm] | $OM_{PS}$ [MNm] |
|---|---|---|---|---|---|---|
| IEA-15-240-RWT [84] | 240 | 1478.6 | 2425.8 | 92.97 | 594.4 | 594.4 |
| MED15MW_240 | 240 | 1324.4 | 2244.2 | 91.46 | 569.7 | 569.7 |
| MED15MW_270 | 270 | 1542.6 | 2521.5 | 98.72 | 682.1 | 650.4 |
| MED15MW_300 | 300 | 1769.9 | 2818.2 | 106.22 | 803.9 | 737.9 |
| MED15MW_330 | 330 | 2005.8 | 3134.2 | 113.97 | 936.9 | 833.2 |
| IEA-22-280-RWT [85] | 283 | 1574.0 | 2769.5 | 117.10 | 784.4 | 784.4 |

$$H_{COM} = \frac{0.4*L_T*M_T + H_{HUB}*M_{RNA}}{M_{tot}} \tag{17}$$

From Table 5 it is apparent how an increased $D_R$ leads to a higher center of mass. In a floating context, this increase is particularly relevant as it affects the overturning moment of the turbine. In addition, Table 5 shows a difference in $M_{TOT}$ and $H_{COM}$ between the 15 MW RWT and the MED15MW_240. In fact, while the IEA reference turbine is a result of a full aeroelastic design, for the proposed turbine the mass scaling relationships mentioned in this section have been utilized. This allowed a fair comparison between the new WT designs.

### 3.2.3. Floater

The floating foundation is designed to keep the installed turbine stable and resist the external actions of the wind and waves. In addition to being able to resist dynamic wind and wave-induced moments, the substructure must be able to resist static forces. Aerodynamic rotor loading is a large part of these overturning forces. As the platform inclines, however, the turbine acts as a reversed pendulum on the structure, and weight forces also tend to overturn the structure. In this respect, the higher the turbine mass and the higher the center of gravity of the turbine, the higher the gravity-induced overturning moment is. While the effect of the component weight cannot be overcome, a reduction of overturning moment can be achieved by reducing peak aerodynamic thrust through the use of peak-shaving. As shown in Table 4, peak shaving can reduce overturning moment significantly, with reductions that range between 5 and 11 % on the current test cases.

The semisubmersible floating platform has been adopted due to its improved stabilization properties and easy installation with respect to the other floaters. The adopted semi-sub geometric configuration consists of three vertical steel columns, interconnected by horizontal pontoons. These columns are partially submerged to provide buoyancy, while the pontoons enhance structural integrity and provide heave damping. The central deck, supported by the columns, houses the WT.

The decrease of WTs' specific power results in the redesign of floating support structures able to deal with enhanced masses and overturning moments. To this end, while scaling laws, which allow for the determination of floater mass from variation in high-level parameters do not exist yet in the industrial field, some approaches have been proposed in the literature. The upscaling method proposed by Wu et al. [88] for semi-submersibles focuses on scaling the pitch restoring stiffness proportionally to maintain the maximum static pitch angle. This stiffness is derived from considering the waterplane area moment, submerged volume, buoyancy, and position of the center of gravity. Two distinct scaling approaches are compared to increase the moment of the waterplane area. The *Distance & Radius Scaling* method simultaneously scales both the column radius and the distance between columns using the same scale factor, while the *Distance Scaling* method adjusts only the distance between columns. Key observations include that increasing column radius increases platform mass and the heave natural period, while increasing column distance elevates the center of gravity and metacentric height but slightly reduces the heave natural period. Design adjustments in the 15 MW reference system mitigate these effects by increasing ballast mass to lower the center of gravity and increasing added mass to lengthen the heave natural period. Despite the accuracy of this method, it implies the geometrical design of the platform. Roach et al. [89] developed an upscaling model based on generalized scaling relations. The methodology consists of a variation of the platform geometric parameters, constraining the platform pitch angle under rated wind turbine thrust, and identifies key scaling trends: platform dimensions scale by a factor of 0.75, while steel mass scales by a factor of 1.5, assuming constant wall thickness. Unlike prior studies focused on specific designs, this approach provides scalable relations applicable to other triangular semi-submersible platforms with three outer columns and a centrally mounted turbine. However, this iterative approach involves the adoption of a complete hydrodynamic model. In their work, Sergiienko et al. [90] resumed the standards [91,92] and best practices [93,94] for the design, construction, and maintenance of FOWTs, identifying the main technical parameters: floatability, maximum roll

and pitch angle, freeboard height, minimum draught, and dynamic response to wind and waves. One of the critical design criteria for ensuring the stability of a semi-submersible platform during wind turbine operation is the ability to generate sufficient restoring moments to counteract pitch and roll motions. To prevent the platform from exceeding the maximum allowable static angle of inclination under the largest rotor thrust, the hydrostatic stiffness in pitch and roll must meet the overturning moment, which is mainly caused by weight and aerodynamic thrust.

To this end, in this work, an approach similar to Ref. [90] has been adopted. For semi-sub platforms, the total restoring stiffness in pitch is predominantly governed by the contribution from the waterplane area. This contribution can thus be associated with the overturning moment of the upscaled turbine to quantify the resulting increases in mass and costs. As floating wind turbines are a novel technology, mature cost models for the floating substructures have not yet been developed. From this point of view, the wide variety of existing foundation designs introduces additional challenges. Therefore, the IEA 15 MW and IEA 22 MW RWTs are used to develop the cost and scaling functions, as both machines are installed on a steel four-column semi-submersible foundation. In addition, the geometry of the IEA 22 MW foundation was determined through an optimization process using the IEA 15 MW design as a baseline [95]. While the external geometry of the floaters has been carefully studied, less consideration has been put into the structural design of the foundations, as they have not been designed in detail. Both the IEA 15 MW [96] and IEA 22 MW FOWTs [97] feature steel columns of 50 mm in thickness and box-shaped pontoons with a wall thickness of 40 mm, which connect the main columns to the central one. The four columns are also connected via steel trusses above the waterline with a wall thickness of 20 mm. Once the wall thickness and the floaters' external shapes are known, it is possible to compute the steel mass for the columns, pontoons, and braces. The cost is obtained by multiplying the component weight by the manufacturing cost of the stiffened columns of 3120 $/t [98] and of 6250 $/t for pontoons and trusses. These values account for raw material costs and manufacturing but do not include transportation costs [98]. According to the authors' knowledge, the maximum OM is available only for the 15 [84] and 22 MW [85] RWTs proposed by the IEA. To this end, due to a lack of additional data, a linear relationship between OM and the platform mass ($M_F$) has been developed as in Eq. (18):

$$M_F = 0.009 * OM - 1157984.96 \tag{18}$$

Fig. 7 shows the comparison between the new FOWTs and the RWTs in terms of mass. Despite the same rotor-swept area and thrust, it is apparent how the correlation results in a mass decrease from the IEA15-MW-RWT to the MED15MW_240. This is due to the reduced OM already discussed and shown in Table 4. Furthermore, the effect of peak shaving is clear in this image. The adoption of an active pitch control strategy to mitigate the thrust resulted in mass decreases that range between 6 % and 13 %.

The same approach has then been adopted to correlate overturning moment and platform cost. To this end, a linear relation between the semi-sub costs ($C_F$) and the platform's mass has been formulated as in Eq. (19):

$$C_F = 2.143 * M_F + 7689597.25 \tag{19}$$

The lack of abundant publicly available cost data for floating foundations is a limiting factor of this study. Nevertheless, the methods adopted to estimate the cost and mass of the IEA 22 MW and IEA 15 MW floaters are aligned with the current state-of-the-art. Fig. 8a shows a comparison between the masses of the semi-sub floaters available in literature (blue dots) and the ones estimated in this study. Despite the relevant amount of data, the values of the overturning moment that the platform has to balance are not available, and correlating these two parameters is not possible. In addition, many datasets do not include cost, as the scarcity of data shown in Fig. 8b demonstrates. Focusing once more on Fig. 8a, an increase in WT swept area is inherently related to an increased overturning moment and thus to heavier floaters. However, this plot shows how technological progress resulted in lighter platforms. The right area of the chart includes recently developed demonstrators or concepts, such as the platforms for the IEA 15 and 22 MW in red, which experience lower estimated masses with respect to WT's nominal power and rotor diameter. Concerning floater costs, Fig. 8b shows the differences between the proposed designs (orange), the literature data (blue dots) and the IEA references wind turbines (red). Information gathered during discussions with industry members, including project developers, consultants, and hull manufacturers is summarized in the shaded areas in Fig. 8b. According to such industry insiders, the cost of European-manufactured steel hulls, represented by the green-colored ellipsis, is now more than double that of the Chinese-manufactured floaters, which are currently the most competitive on the market. However, these costs are based on projections of a limited number of produced units. The cost estimations performed in this work assume the development of the technology combined with the large-

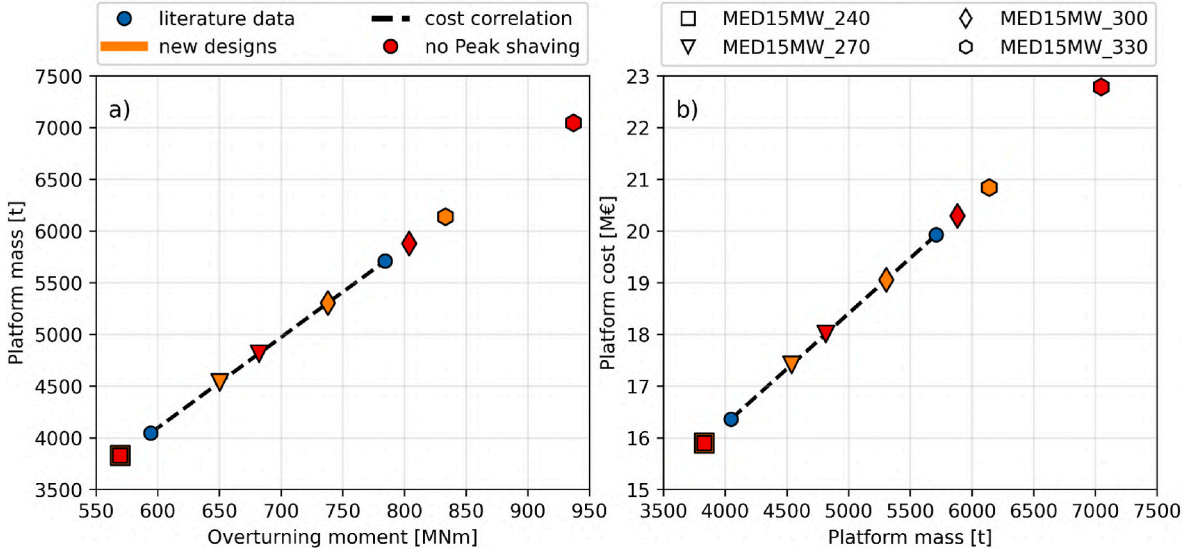


**Fig. 7.** (a) platform mass - literature and proposed data relying on the introduced correlation. (b) platform cost - literature and proposed data relying on the introduced correlation. Red markers indicate platform mass and cost of proposed designs without the adoption of peak shaving.

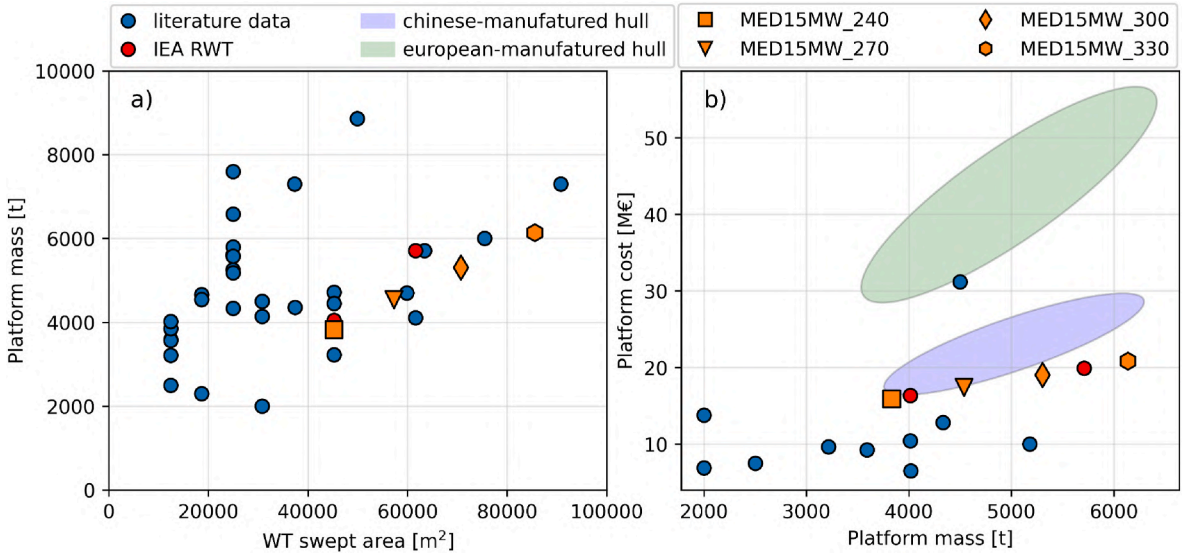


**Fig. 8.** Comparison between the results and literature data for platform masses and costs.

scale commercialization. The data utilized in Fig. 8 are reported in Appendix B.

Delving more in-depth, the marginal cost of the turbine components, as determined using the cost and scaling functions developed in this section, is summarized in Fig. 9. The platform represents about 55 % of the whole turbine cost. This is consistent with a reduction of about 5 % of the total cost due to the implementation of peak shaving.

Focusing on the economic impact that the swept-area increase has on the cost of the single component, it is apparent how, while the weight of most of the WT components decreases with respect to the total cost, the impact of the rotor and tower increases. This is consistent with the assumptions adopted in the cost scaling method proposed, where the rotor price shows the highest sensitivity to the size. However, while the impact of peak shaving has been considered in terms of its effect on wind turbine performance, it has not been considered in terms of its potential to decrease the rotor weight. In fact, the reduction of maximum thrust on blades may lead to a reduction in structural material in the rotor, due to the lower loads, and thus to a CAPEX reduction. No cost and scaling function that accounts for the effect of peak shaving on rotor mass has been found at the current stage and this effect can currently be considered only by performing a full aero-elastic design. The results presented in this study can therefore be assumed to conservatively favor the smaller rotor designs, which feature less peak-shaving, from an economic point of view. Finally, looking at Fig. 9, insights into how to reduce the WTs CAPEX can be provided. It is apparent that the floater has the highest weight on cost. While the other components have already experienced a large deployment, both in onshore and offshore environments, floating platforms represent the less developed and widespread technology, counting only a few demonstrators. To this end, due to its large share of total costs, lowering floater costs has the potential to drive down overall FOWT LCoE.

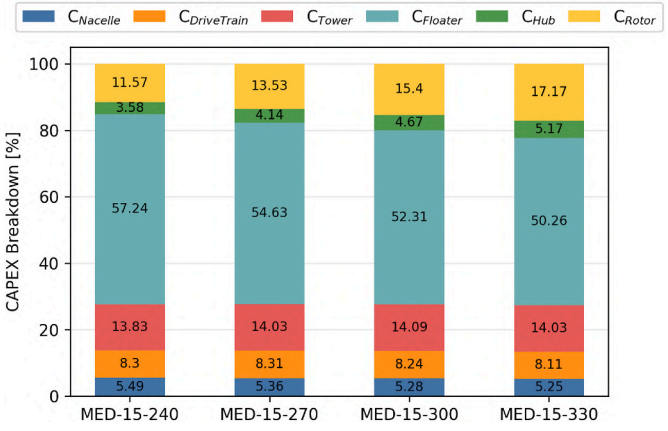


**Fig. 9.** WT CAPEX breakdown for the designed aerogenerators.

### 3.3. OPEX increase

Besides the increased capital requirements due to the larger swept areas, as rotor size increases, OPEX is also expected to rise [9,19,35]. The adoption of larger rotors with more flexible blades introduces relevant alterations in the aeroelastic behavior of the WT, resulting in larger mechanical stresses. These enhanced loads have the potential to activate novel failure mechanisms within the turbine, leading to variations in failure rates and necessitating the implementation of alternative and potentially more expensive maintenance strategies [99]. However, few research efforts have been made on analyzing the impact of the specific power decrease and rotor upscaling on operational costs [86]. In this study, the approach proposed by Mehta et al. [37] has been adopted. Specifically, operational costs encompass various factors such as insurance, logistics, and other associated expenses, while maintenance costs include both preventive and corrective maintenance for the turbine and the balance of plant. While the total OPEX depends on multiple variables unrelated to the WT swept area per se, such as number of turbines and rated power, vessel costs exhibit a linear scaling relationship with the rotor diameter [100] to mimic the costs faced during actual operation of floating offshore systems, which require different vessel types and times to perform repairs as rotor size increases. To this end, the DTU scaling model has been modified in order to assess these OPEX variations by including a multiplication factor estimated through the ratio between the reference and the actual rotor diameter as in Eq. (20):

$$OPEX_{NEW} = OPEX_{BASE} * \frac{D_{NEW}}{D_{BASE}} \tag{20}$$

where the subscripts new and base represent the turbine with the increased diameter and the reference one, respectively.

## 4. Optimization model

In this study, the TopFarm wind farm analysis and optimization framework [101], developed by the DTU, has been adopted to determine

the optimal wind turbine and cabling layout that minimizes LCoE in a specific location. TopFarm enables comprehensive and efficient exploration of design variables while balancing conflicting objectives such as maximizing energy production and minimizing costs, by implementing optimization strategies. The optimization model, focusing on the intra-farm wake loss calculation strategy, IA cable layout optimization, and the definition of the objective function and constraints is presented in this section.

### 4.1. Power production assessment

PyWake [102] is a Python-based wind farm simulation tool designed to model the performance of wind farms under various conditions. It has been adopted to estimate the AEP of a WF layout in a specific site. Several key factors collectively influence the AEP of a WF layout; the wind resource, turbine characteristics, and the interactions between turbines within a wind farm. The wind farm model integrates the site information, wind turbine model, and wake model on the entire wind farm computing key metrics such as the annual energy production (AEP), wake losses, and turbulence intensity for the specified wind farm layout and wind resource conditions.

The installation site determines the long-term average wind speed, which is described using Weibull curves, and the wind rose, which specifies the directionality of the wind. As specified in section 2.3, the long-term statistical representation of the site is obtained using 1-h average data from the ERA5 reanalysis database [103] at 100 m above sea level. Additional environmental factors, such as surface roughness and terrain effects have been neglected due to the offshore installation. The average wind speed is scaled from 100 m to the turbine hub-height using a power law with an exponent of 0.11, typically adopted in an offshore environment [104]. The adoption of a statistical approach ensures good accuracy for the calculation of the LCoE, and the upgrade to a time-dependent strategy would only have resulted in a computational cost increase.

The wind turbine is modelled through the turbine's power curve, which relates wind speed to power output and the thrust curve, which determines the extent of momentum extraction by the turbine and, consequently, the intensity of the wake for a given wind speed.

The wake model describes the time-averaged behavior of the wake generated by each turbine, including how it expands and impacts the downstream WTs, predicting the velocity deficit and turbulence intensity within the wake. In this work, the Bastankhah model has been adopted [105]. This advanced analytical wake model describes the wake as a Gaussian profile, capturing a more realistic distribution of velocity deficits and turbulence [106] with respect to simpler approaches [107]. The "LinearSum" model has been adopted [108] to estimate the effective wind speed at each WT location within the farm given by the superposition of different wakes. To account for partial overlapping between a downstream rotor and an upstream wake, the Gaussian overlapping model available within PyWake has been adopted, in accordance with existing guidelines [109]. Finally, the turbulence models in PyWake are utilized to estimate the added turbulence in the wake from one aerogenerator to downstream WTs within the wind farm. Pywake's "GCLTurbulence" has been adopted herein [110].

### 4.2. IA cables layout

Two different strategies can be used in TopFarm to determine the total inter-array cable length: the simplified approach proposed in Ref. [111] and the detailed tool Edwin [112]. The two approaches differ in several key details.

The basic optimization model adopted is a reimplementation of the *Travelling Salesman Problem* (TSP). It is representative of the behavior of a salesman who must visit multiple locations while minimizing travel distance. The adoption of this approach is reasonable, especially for onshore wind turbines, where IA cables often follow maintenance roads connecting the turbines. Once the grid optimization is performed, the cable costs are estimated by multiplying the specific costs by the total length of the IA network. In addition to the TSP assumption, the electrical cables used to connect the wind turbines within a wind farm are designed to carry specific voltage levels, which define the maximum number of turbines that can be connected per cable. However, such design constraints that introduce a higher level of complexity are not considered in Ref. [111], and the model assumes idealized cables capable of transmitting all the electricity produced by the connected turbines.

As an alternative, Edwin relies on the Esau-Williams heuristic algorithm developed by Souza de Alencar [113]. The algorithm minimizes the total cable length by identifying sub-optimal solutions that closely approximate exact solutions. The Esau–Williams heuristic is applied by constructing a minimal-cost spanning tree for a graph with designated roots, nodes, and capacity constraints. In this study, the offshore substations serve as the roots of the spanning tree, while the FOWTs act as the nodes as shown in Fig. 10b. The algorithm permits sub-branches along a given string while ensuring that the maximum number of nodes per string is not exceeded. Edwin includes actual cable constraints, such as the maximum voltage allowed by the electrical network and the section of the cables, defining the number of WTs that can be connected. Additionally, it enables the optimization of the location of the offshore substation within the wind farm.

Both approaches have been tested during the model build-up phase. According to the preliminary results, Edwin leads to relevant cost savings, with cable length decreases up to 50 km. In addition, despite the increase in computational burden, the resulting IA cable layout is more realistic. To this end, this tool has been included in the wind farm layout optimization framework for the analyses performed.

Concerning the IA cable specification, the same component adopted in Ref. [47] has been chosen. Specifically, cables characterized by a cross-section of 800 $mm^2$ and a nominal capacity of 90 MW have been selected as a valuable option, allowing for the connection of a maximum of 6 FOWTs per cable. This, combined with the spatial distribution of the aerogenerators, resulted in six cables connecting six WTs and five cables connecting five WTs for all the analyzed configurations.

### 4.3. Objective function

This study utilizes LCoE as the objective function for the optimization problem. LCoE provides a holistic approach by accounting for all elements impacting generation costs, such as CAPEX and OPEX. It is calculated as the ratio of the total discounted costs incurred over the facility's lifetime (n) to the total discounted energy output ($E_{prod}$) over the same period. As the electricity is derived from a renewable source, fuel costs are not included, as shown in Eq. (21), where *i* represents the interest rate:

$$LCoE = \frac{\sum_{t=0}^{n} \frac{CAPEX_t + OPEX_t}{(1+i)^t}}{\sum_{t=0}^{n} \frac{E_{prod,t}}{(1+i)^t}} \tag{21}$$

### 4.4. Wind farm optimization algorithm

The optimization process in this study is driven by the capabilities of the TopFarm framework, which leverages computational tools to solve the complex, multidisciplinary problem of wind farm design. At its core, TopFarm utilizes the OpenMDAO library [114], a powerful open-source framework developed for multidisciplinary optimization, to link the modules within the optimization tool. The core of the optimization process is shown in Fig. 10. The optimization framework proposed operates as an iterative process, as shown in Fig. 11, aimed at minimizing the LCoE. In each iteration, a new WF layout is tested. The process begins by estimating the Annual Energy Production (AEP) of the

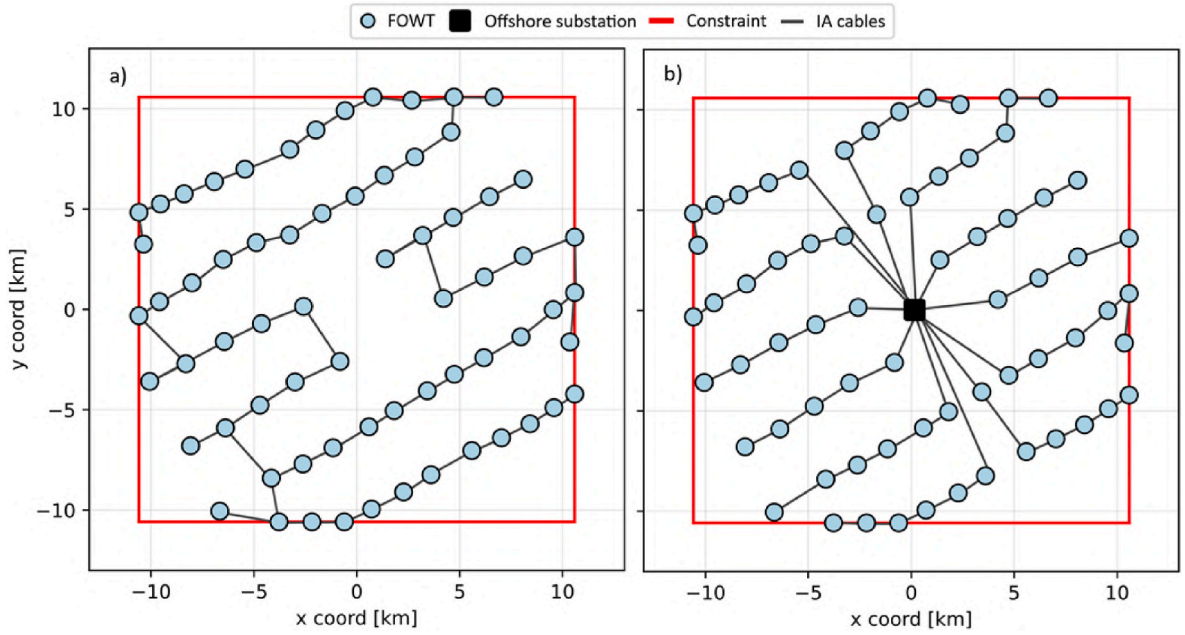


**Fig. 10.** Optimal IA cable layout obtained with the TSP reimplementation (a) or Edwin (b).

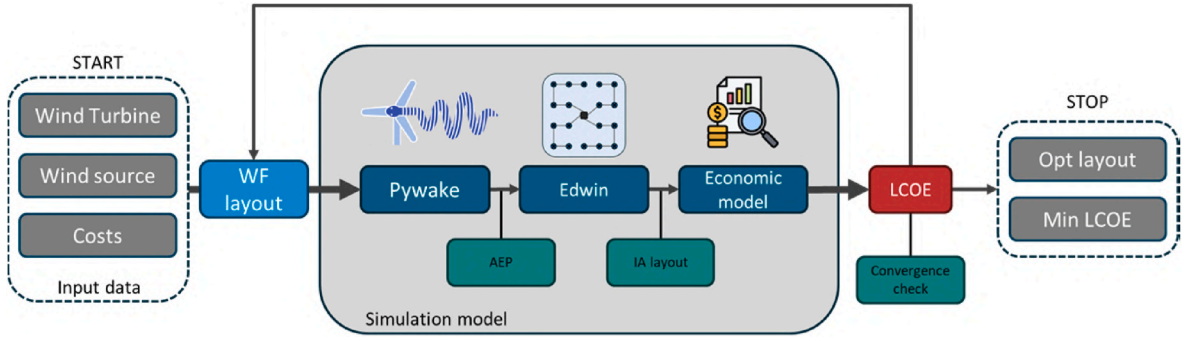


**Fig. 11.** Schematic representation of the optimization model.

proposed layout using the PyWake library. Then the optimal layout of the inter-array cables is determined by solving the sub-optimization problem described in the previous section. This problem focuses on minimizing the total cable length while the location of the WTs is fixed. Once the cable layout is optimized, the framework estimates the CAPEX and OPEX for the current wind farm configuration using the cost models presented in detail in section 3. This leads to the calculation of the LCoE as a final step. The newly calculated LCoE is then compared with the value obtained in the previous iteration. This comparison continues across iterations until the convergence criterion is met. Specifically, convergence is reached when the change in the objective function between iterations is below the predefined tolerance value, set at $1*10^{-8}$.

In this study, the "Constrained Optimization BY Linear Approximations" optimization algorithm (COBYLA) has been employed, a local-search method that does not rely on gradient computation. COBYLA is a gradient-free optimization algorithm that uses linear approximations to solve non-linear, constrained optimization problems. This makes it particularly well-suited for problems involving discontinuities or non-smooth objective functions, such as those arising from the interaction of turbine wakes or discrete design variables like turbine selection.

### 4.5. Constraints

The optimization model used in this study encompasses several essential constraints to ensure that the wind farm design is both feasible and aligned with technical, regulatory, and operational requirements. One of the key constraints is the minimum turbine distance, which ensures the required separation between turbines needed to preserve structural integrity. This distance is typically defined as a multiple of the turbine $D_R$, following industry standards to balance energy yield with turbine durability and operational reliability. Specifically, 4 $D_R$ has been set as the minimum WT spacing, according to the guidelines proposed in Refs. [115–117]. Fig. 12 shows a schematic representation of the minimum IA distance for floating offshore wind turbines. The report [118] published by the consortium composed of BVGA associates, Catapult, The Crown Estate, Crown Estate Scotland, and Floating Offshore Wind Centre of Excellence, presents a detailed description of the best practices for FOWTs. Specifically, it states that the WT displacement allowed by the mooring lines corresponds to around 35 % of the sea depth of the installation sites. Therefore, taking the IEA-15-240-RWT and a sea depth of 160 m as a reference, the allowed motion is equivalent to 0.25 $D_R$ for each WT, and the distance between the WT and the column where the mooring is connected ranges between 0.2 $D_R$ and 0.3 $D_R$ [119]. It is apparent that the minimum distance needed is about two $D_R$, which reaches the amount mentioned in Refs. [115–117] with an appropriate safety factor.

The wind farm design is also restricted to a predefined allowed sea lot for installation, reflecting the geographic and regulatory limitations

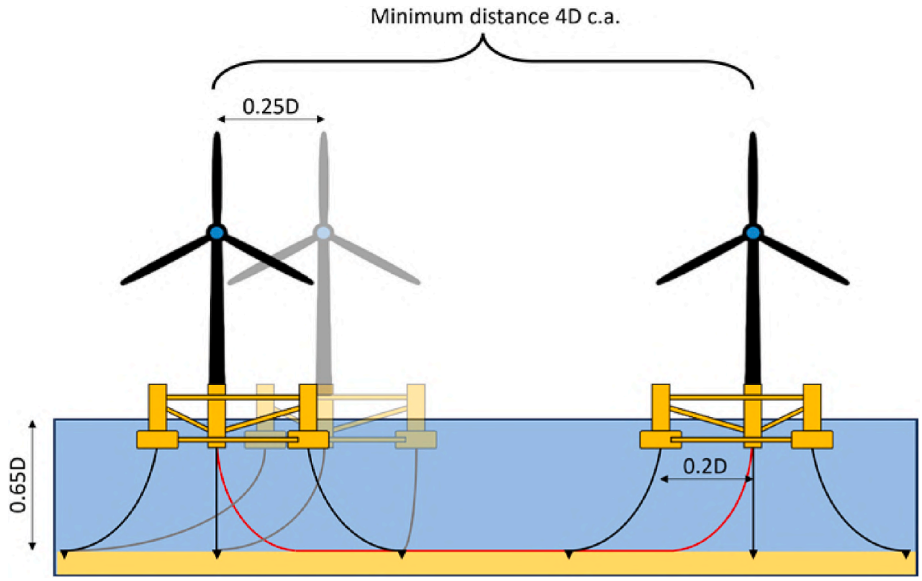


**Fig. 12.** Scheme for minimum IA distance between WTs.

of the site. Although not specifically evaluated in this study, and despite constraining a wind farm to a specific area may not lead to the global minimum LCoE, wind farms are often assigned specific sea lots. These constraints are generally defined in order to account for neighboring environmental exclusion zones, land-use policies, or proximity to infrastructure like shipping lanes or residential areas. In this study, the wind farms are constrained to a 450 $km^2$ lot. While a rectangular sea lot may affect the WT location with respect to the prevalent wind direction, a squared one enables a comparison *ceteris paribus* between the different case studies proposed. Although true independence from wind directionality would have been achieved by using a circular installation area, this shape has never been adopted for offshore wind farms, which are generally polygon-shaped according to the authors' knowledge.

## 5. Results

This section makes use of the optimization model synthesized in Section 4 to critically assess the potential of LSP rotors in the four installation areas in the Mediterranean Sea that were selected as representative of those average-wind speeds areas that are under study worldwide to expand FOWT technology. It is worth remarking that the outcomes presented in this section refer to the 1 GW wind farm layout resulting from the proposed holistic optimization model and are therefore thought to represent the most realistic estimations at hand for possible industrial application of the technology.

### 5.1. Technical results of the optimization

Fig. 13 shows the energy production potential in the four selected sites and apparently demonstrates how the strategy adopted for the reduction of the specific power increased the AEP in all cases. However, the variation (Δ) of AEP with respect to the one obtained with the 240-m diameter rotor is affected by the Weibull curve of the specific site. In fact, while Lyon shows the most promising wind speed distribution (Fig. 2) and the highest AEP for all the tested rotor diameters, it experiences the lowest benefits from the increase of swept area (Fig. 13b). On the other hand, while Cyprus is characterized by the worst wind source (as testified by the low AEP in Fig. 13a, it is the site experiencing the highest improvements. These trends are consistent with the assumption behind this work, which promotes the installation of larger blades to enhance wind energy exploitation at the lower wind speeds in the Weibull distribution.

Additionally, the distribution of the AEP with respect to the wind speed improves the understanding of these results. Fig. 14 shows the energy production potential of the 1 GW wind farm in the French and Cypriot sites for the MED15MW_240 and MED15MW_330, respectively.

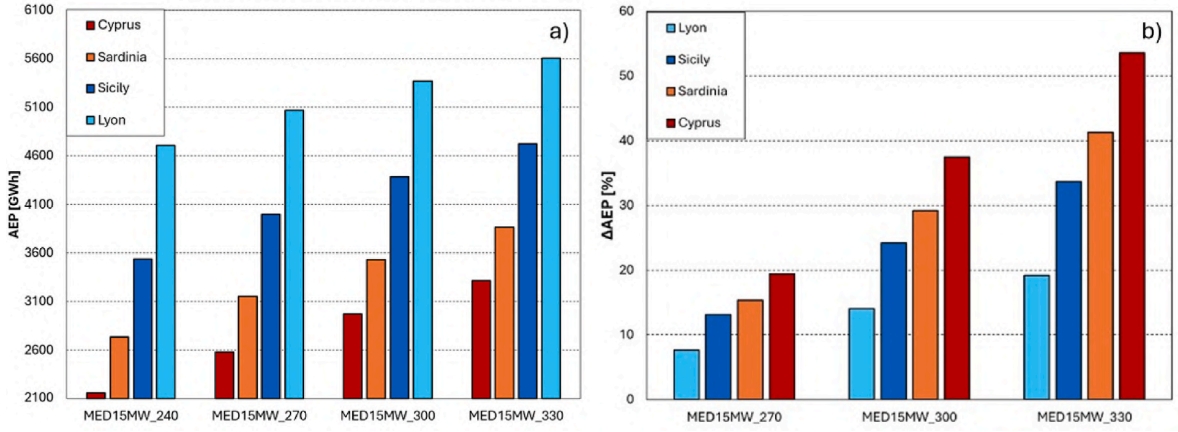


**Fig. 13.** Comparison between the AEP and the AEP variation in the different installation sites for the new aerogenerator designs.

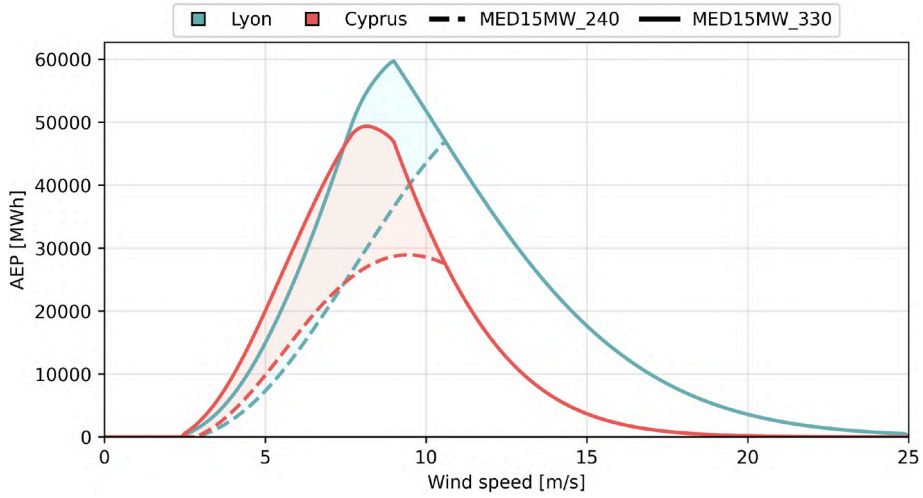


**Fig. 14.** Comparison between the AEP distribution in the French and Greek installation sites for the MED15MW_240 and MED15MW_330.

While the AEP of the French case is higher for both aerogenerators, the installation site in Cyprus benefits more from the specific power decrease, as the opportunity for AEP improvement are greater the more time the turbine spends below rated power.

Further considerations can be made by looking at the wind speed deficits induced by wakes. As shown in Fig. 4, lower specific power leads to higher maximum thrust at reduced wind speeds, resulting in stronger wakes. Additionally, larger rotors extend the length of the wake, increasing its area of influence. These effects are depicted in Fig. 15, where the difference in the downwind speed deficit between isolated MED15MW_240 and MED15MW_330 rotors is shown. The wind speed deficit contour, estimated by imposing the same thrust for both turbines, shows a more severe velocity decrease with the MED15MW_330, depicted by the larger dark blue area, which is extended further from the rotor position, as highlighted by the dashed vertical line.

Such an effect has the direct consequence of affecting the optimal distance between the turbines. Fig. 16a shows the comparison between the optimal wind farm layout obtained for the wind farm located in Sicily with the MED15MW_240 (light blue) and the MED15MW_330 (blue) WTs. It is apparent how the increased impact of wake losses, which increase from 3.5 % to 3.7 %, respectively, in the optimized configuration, induced by the larger swept areas results in an increased optimal spacing between turbines. It is worth noting that the optimal solution features increased turbine spacing despite the increasing cable costs, as the increase in AEP offsets the increase in CAPEX. Furthermore, starting from the initialization position (grey), in both cases, the orientation of WTs clusters resulting from the optimization process is N-NW. This can be justified by the wind source in the Sicilian installation site, where the prevalent wind direction corresponds to the orientation of the farms (see Appendix A). Particularly noteworthy is the comparison between the initial and final wind farm layouts. In fact, the choice of a starting configuration close to the optimal one, estimated by the authors via sensitivity analyses in previous works [], sensibly reduced the computational time required for the optimization.

The same trend can be observed for Cyprus in Fig. 16b, where the prevalent wind direction is W-SW. In this installation site, the reduced global IA cable length of about 5 % with respect to the Italian case suggests a lower average distance between turbines. This is again consistent with the wind speed distribution of Cyprus, whose average velocity is shifted towards lower values. Concerning wakes, the higher swept area leads to an increase in losses from 3.5 % to 4 %. The higher upper bound compared with the one in the Italian site can be justified by looking at the thrust curve of the turbines and at the wind speed distribution. The lower average wind speed experienced in Cyprus -equivalent to 5.6 m/s-is closer to the velocity that maximizes the thrust for the MED15M_330, leading to a stronger impact of wake losses.

This result, however, depends on the boundary conditions of the optimization. For instance, given the reliance on IA cables, whose impact on LCoE has been estimated at about 5 %, variations in the cost of this component can significantly affect the overall economic feasibility.

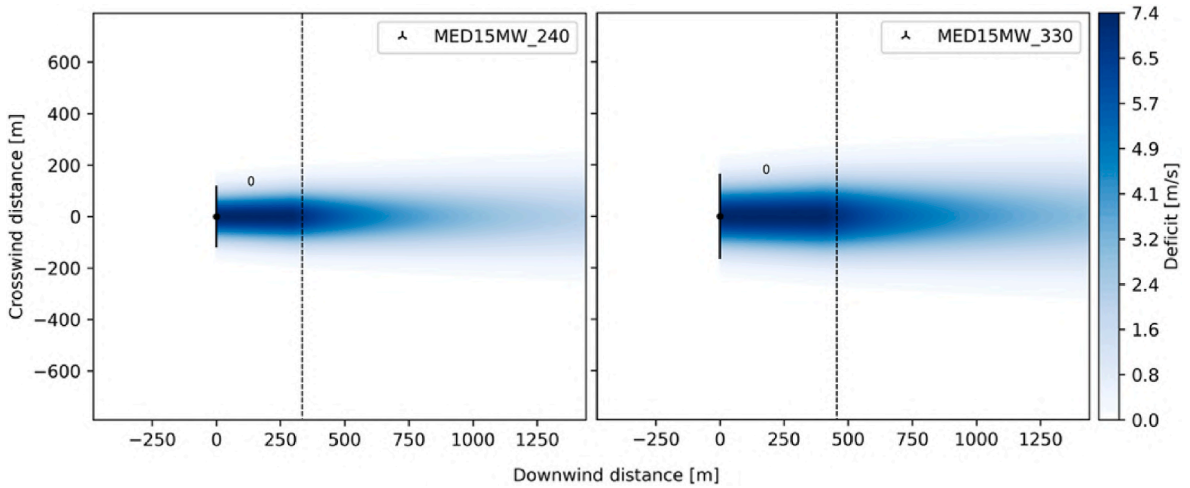


**Fig. 15.** Comparison between the wake effects of the MED15MW_240 and the MED15MW_330 WTs.

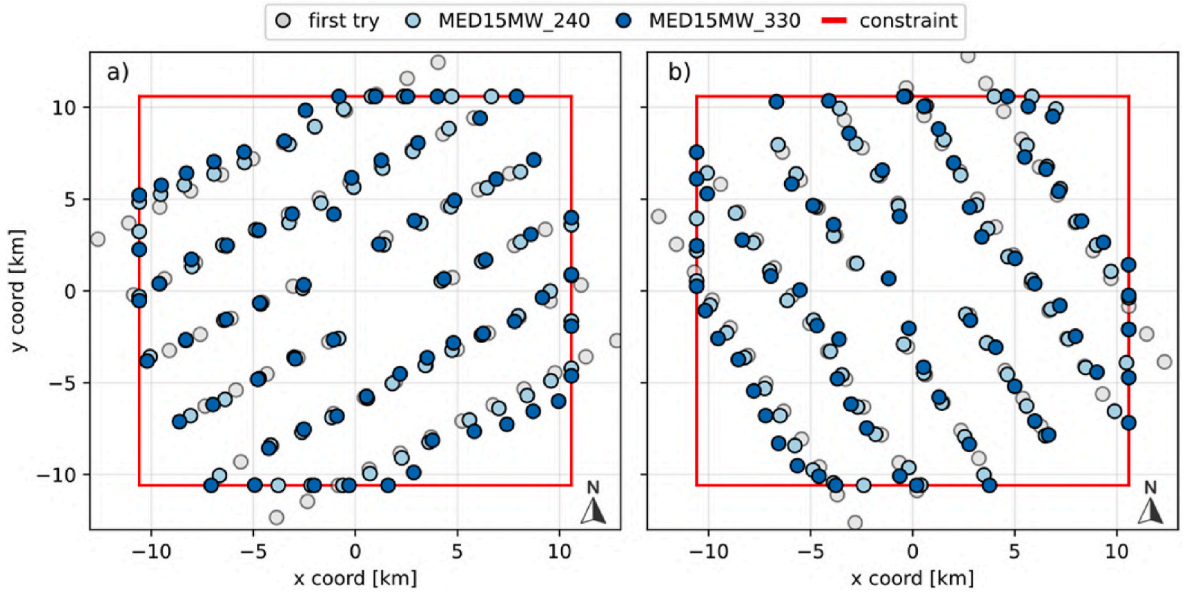


**Fig. 16.** Comparison between the optimal layout obtained in Sicily (a) and Cyprus (b) for the wind farms with the MED15MW_240 and the MED15MW_330 WTs.

Therefore, a sensitivity analysis of the cable price, decreasing this value from 750 to 500 €/m, driven by market fluctuations or project-specific factors, has been performed in order to explore a wider design space and evaluate new techno-economic trade-offs. This economic range has been defined by subtracting 30 % from the reference value, identified as 750 €/m. Decreased cable costs per km result in a lower CAPEX with the same WF layout.

On the other hand, enhanced spacing between WTs leads to reduced wake losses. Specifically, a decrease in inter-array cable cost allows for an increased distance between the WTs, as shown in Fig. 17, leading to the reduction of wake losses and thus higher AEP. Despite the global increase in the length of the cables, spanning from 14 to 30 km depending on the rotor diameter, the CAPEX for the electric infrastructure has experienced a decrease due to the new optimal layout.

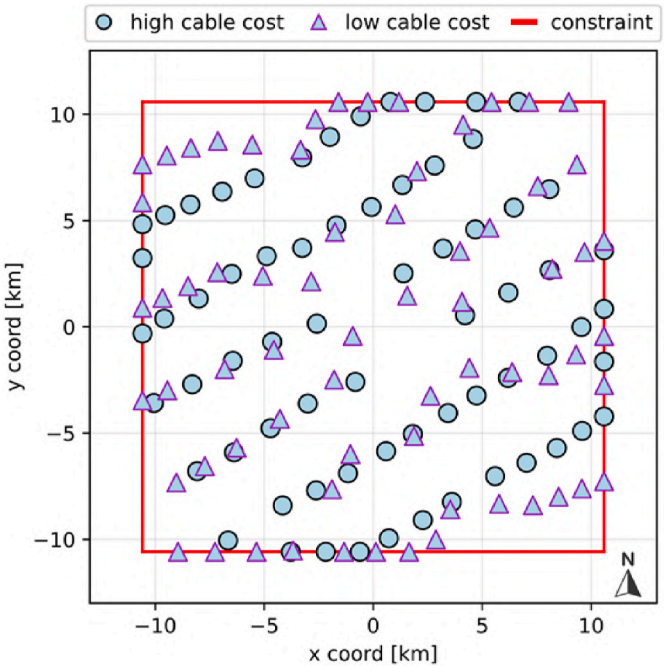


**Fig. 17.** Comparison between the optimal layout obtained in Sicily with two different IA cable costs for the MED15MW_240.

This, combined with the higher energy production potential, resulted in a lower LCoE.

### 5.2. Environmental analysis

The WTs' environmental impact is gaining momentum in the scientific community and the public interest and, according to experts in the field, this will be a criterion for upcoming tenders [120,121]. However, a complete life cycle analysis would require a detailed design of the system, including the installation and decommissioning procedures, which is completely site-dependent and can hardly be generalized in a global assessment as the one proposed here. To this end, a simplified approach for the evaluation of the environmental impact of floating wind farms has been proposed, relying only on the amount of steel required by WTs and floaters. According to Table 6 and Figs. 6 and 7, larger swept areas lead to increased masses and thus to enhanced steel consumption. This results in higher $CO_2$ emissions that are not necessarily balanced by the increased AEP during the WT lifetime. Table 6 shows that the amount of steel needed for each turbine-floater assembly varies significantly with the specific power, leading to a $CO_2$ emission increase that ranges between 20 and 60 % with respect to the 240-m diameter rotor when a carbon footprint of 1.85 t of $CO_2$ per ton of produced steel is adopted [122]. On the other hand, the enhanced AEP resulting from the increased swept areas (Fig. 13) leads to a wind farm's carbon footprint reduction. Focusing on the Italian electricity mix, the average carbon emissions per MWh of electricity produced in 2024 are about 270 kg/MWh, consistent with a share of 49 % of renewables [123]. While the deployment of the MED15MW_330 results in an increased carbon payback period (CPBP) -from nine months of the MED15MW_240 to about one year in the installation site in Sicily-the environmental benefits on the whole lifetime of the wind farm are relevant. Assuming a constant carbon emission for the whole plant lifetime, the 30 years of operation of the wind farm in Sicily can help to avoid the emissions of more than 38 Mt of $CO_2$, with the WT with the highest swept area, corresponding to an improvement of more than 33 % with respect to the base 15 MW WT. Fig. 18 shows the comparison between the $CO_2$ saved by the new WTs designs in the different installation sites. It is apparent that the most impactful factor is the carbon emission per unit of produced energy of the specific country. The site in the Gulf of Lyon, despite the highest AEP, experiences the lowest emission factor −27 kg/MWh [124] due to the high shear of nuclear energy, and thus

**Table 6**
Steel consumption and $CO_2$ production increase for the single turbine-floater assembly due to higher swept areas.

| Wind Turbine | MED15MW_240 | MED15MW_270 | MED15MW_300 | MED15MW_330 |
|---|---|---|---|---|
| **Steel consumption [t]** | 6100.74 | 7265.11 | 8534.95 | 9917.91 |
| **CO2 emissions [t]** | 11286.36 | 13440.46 | 15789.66 | 18348.14 |

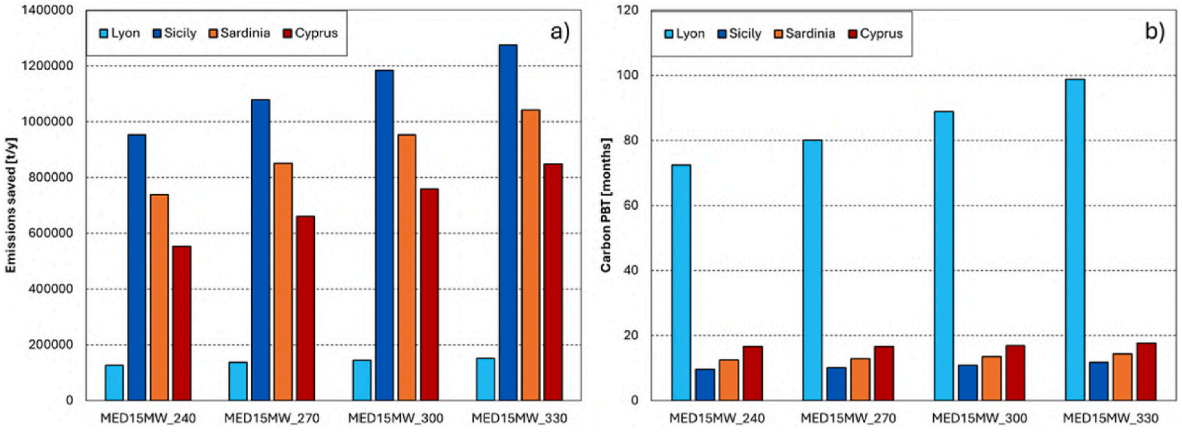


**Fig. 18.** Comparison between the carbon emissions saved and the carbon PBT for the tested WTs in the different installation sites depending on the emission factor of each Country [125].

the lowest saving potential. This results in the highest CPBP, with periods of up to eight years to reach neutrality. However, even in this extreme scenario, the adoption of WTs with lower specific power is beneficial in terms of emissions saved per year. Finally, Fig. 18 also allows for a comparison of the Italian sites. Despite the lower global emissions saved per year, the higher ΔAEP of Sardinia results in an enhanced environmental benefit in the adoption of the MED15MW_330, with a yearly carbon footprint reduction increase of up to 41 % with respect to the base turbine.

### 5.3. Economic results of the optimization

Although the increased swept area impacts positively the capacity factor of the wind farms, and thus their AEP, this study aims mainly to assess to what extent a tailored WT can minimize the LCoE in a specific site by pursuing a trade-off between increased expenditures and the higher AEP. The comparison between Figs. 13 and 19 shows how, while the AEP always rises, the LCoE trend strongly depends on the wind source. The relevant ΔAEP depicted for Cyprus leads to a minimum cost of energy obtained with the WT with the lower specific power. This is consistent with the Weibull of this site, which shows a high amount of energy at the lower wind speeds. To this end, the more the operation curve is shifted towards lower wind speeds, the larger the benefits. Regarding the Italian sites, the wind energy distribution is translated towards higher wind speeds with respect to Cyprus. In these scenarios, the sensitivity analysis to the rotor diameter identifies MED15MW_270 and 300 as the optimal solutions for Sicily and Sardinia, respectively, as shown by the ΔLCoE in Fig. 19b. This is again consistent with the wind resource of the two sites, which shows a higher average wind speed in Sicily than the one in Sardinia. Finally, while the site in the Gulf of Lyon experiences an increase in AEP, the higher CAPEX related to the larger swept area offsets the enhanced production potential, leading to a negative impact on costs. Fig. 19 shows how the optimal situation is represented by the turbine with the reference rotor diameter and further decreases in the specific power result in higher LCoE. This can be justified again by looking at the wind speed distribution in Fig. 2. The Weibull in this site is the closest to Class I, which has been taken as a reference for the design of the IEA RWT with a rotor diameter of 240 m.

IA cable costs affect only the LCoE, without modifying the optimal rotor swept area for the specific site. Fig. 20 shows the comparison between the LCoEs obtained with IA cable costs of 750 €/m (hatched bars) and 500 €/m (solid bars). The hatched bars, representative of the base

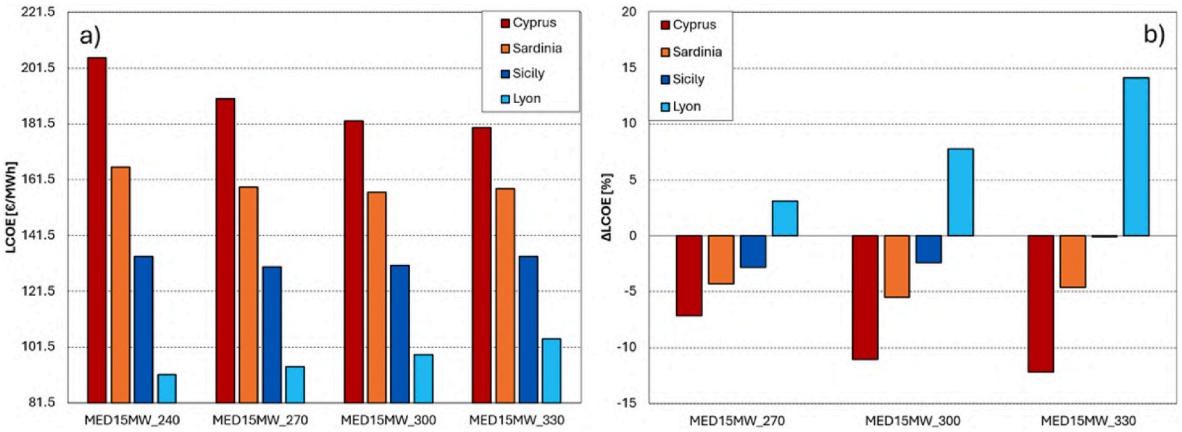


**Fig. 19.** Comparison between the LCoE and the LCoE variation in the different installation sites for the new aerogenerator designs.

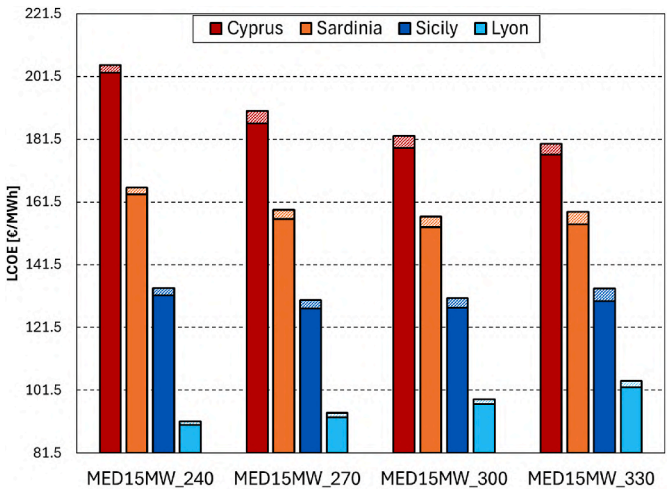


**Fig. 20.** Comparison between the LCoE in the different installation sites for the new WT designs with different IA cable costs.

case study, always exceed the LCoE depicted by the solid bars. When less expensive IA cables are used, the LCoE decreases as a consequence of the lower wake losses and reduced CAPEX. On the other hand, the unchanged optimal WTs emphasize a lack of direct dependency between the IA cable costs and the optimal swept area. From these preliminary results, it has been noticed that the optimal rotor diameter per se is influenced only by the wind speed distribution in a specific site.

## 6. Discussion

The findings of this study underscore the potential of LSP wind turbines as a key technological advancement for regions with moderate average wind speeds, such as those prevalent in many Mediterranean countries. In alignment with the stated objectives, this discussion synthesizes the key findings and provides a broader perspective on their implications.

First, the literature review highlighted a significant gap in current methodologies, particularly the oversimplification in estimating the AEP based solely on wind profiles and hypothetical power curves. As shown in many studies, such approaches risk overlooking complex but critical interactions between turbine design, farm layout, and economic performance. By contrast, the comprehensive approach adopted in this review underscores the necessity of integrating detailed cost and performance drivers, such as wake losses, substructure design, and cabling costs, into early-stage feasibility analyses. In particular, this study clarified that the promise of LSP turbines in moderate wind areas affects not only their aerodynamic efficiency but also their energy system implications [126]. The detailed component-level review revealed how changes in rotor size and specific power influence the mass and cost scaling of rotors, towers, and floaters. These impacts are not independent; for example, larger rotors associated with LSP configurations tend to require taller towers and more robust floating structures, which may offset some of the expected energy gains. However, in the context of moderate wind sites where capacity factors are inherently lower, LSP turbines offer a valuable trade-off by improving AEP without significantly increasing operational expenditures. Despite lower specific power rotors being hampered by higher CAPEX, in fact, several key advantages have been highlighted. By optimizing the WT swept area, despite the increased costs, both the LCoE and the environmental impact of aerogenerators can be reduced. Additionally, this approach leads to higher capacity factors, which may also be beneficial for expanding renewable energy capacity in sea basins with moderate wind speeds and deep waters that have not yet been exploited with conventional offshore wind technology. In addition, lowering specific power increases the availability factor, which is often valuable in energy grids with high penetration of intermittent renewable energy. From this perspective, the results are of interest for future analyses by both policymakers and relevant stakeholders, including energy producers, private investors, and utility companies that could push forward the development of a new generation of rotors tailored for specific markets. Increased investment in this technology could, in fact, not only contribute to renewable energy targets but also help enhance grid resilience and promote sustainable development of regions such as the Mediterranean one. By selecting the Mediterranean Sea as a case study, this study was able to contextualize theoretical findings within real-world site conditions, including variations in wind resource, water depth, and infrastructure availability. This region-specific analysis demonstrated that while LSP FOWTs may not be universally optimal, their strategic deployment in select moderate-wind locations could bridge the gap between current technology limitations and future offshore wind expansion goals.

A comparison between the results obtained in this study and those presented in previous works highlights both the evolution of cost trends and the limitations inherent in certain modeling approaches. For instance, the wind farm specific CAPEX estimated in this work ranges between 3480 and 5100 €/kW, whereas [24] reported a lower range of 3200–4550 €/kW. While the lower bound is in line with the literature, the upper-bound CAPEX found herein is influenced by the use of low specific power wind turbines, which increases CAPEX. Therefore, due to this metric not considering the AEP improvement of the larger rotors, energy production benefits cannot be quantified against their higher capital costs, making a direct comparison with this study [24] challenging.

Further comparison can be made with the work of Serri et al. [67], who reviewed LCoE estimates for wind projects in the Mediterranean Sea. Their reported LCoE range of 63–156 €/MWh aligns well with the present results, particularly for high-wind-resource areas such as Sicily and the Gulf of Lion. Conversely, sites characterized by lower average wind speeds, such as Cyprus and Sardinia, show consistency with the upper bound reported by Martínez and Iglesias [57], where the LCoE can reach up to 250 €/MWh. These parallels support the validity of our modeling framework and highlight the critical role of site-specific wind conditions in determining economic viability.

While the presented model is comprehensive and physically consistent, technical and economic limitations should be acknowledged to contextualize the results accurately. The impact of peak shaving on blade weight has not been considered. A reduction in loads due to peak shaving could result in lighter blades due to the lower aerodynamic loads. However, accurately assessing this effect requires a detailed structural design, which is beyond the scope of this study. Consequently, the results presented here represent a conservative scenario (i.e., additional reductions in LCoE are at hand), that still offers meaningful insights into the proposed solution. Additionally, the impact of turbulence on WT thrust has been neglected, leading to a conservative estimation of wake effects. This simplification may result in an overestimation of wake losses, which would likely lead to slightly improved outcomes if turbulence effects were included. This assumption is adequate for the comparative scopes of the study. Finally, no sensitivity analysis has been performed on the occupied area due to a lack of literature data on costs per unit surface for sea lots. As a result, any potential improvement in surface efficiency in terms of energy output per square kilometer of sea surface, would favor larger, more productive rotors, under the constraint of a set permitted sea lot and set number of permitted turbines of set specific power.

Concerning economic assumptions, no sensitivity analysis for the costs of platforms and other ancillary components, such as export cables and offshore substations, has been conducted. For all these components, the cost scaling models described in the methods section have been consistently applied. These models are based on established industry standards, empirical data, and literature values, ensuring a realistic and standardized approach to cost estimation across the project. Any fixed

cost increases or decreases would uniformly affect all turbines and installation sites analyzed, thus preserving the comparative nature of the study's conclusions. Therefore, variations in these costs could introduce uncertainty into the LCoE estimations, but they would not change the optimal turbine configuration for the installation sites. On the other hand, modifying the platform cost correlation by increasing or decreasing the dependency of the expenditure by the swept area may affect the optimal WT for a specific site. However, according to the limited amount of data available in the literature, arbitrary adjustments to the relation presented in Section 3 would be arbitrary, and was thus considered irrealistic.

Finally, while more complex economic metrics, such as the Cost of Value of Energy (CoVE) [127,128], are increasingly explored in academic literature and energy tender evaluations, we opted to use the LCoE due to its widespread adoption and suitability for comparative analyses. In this study, LCoE was particularly appropriate as different turbine configurations have been compared to evaluate the benefits of larger rotors. Metrics like CoVE require time-dependent simulations of wind power output and detailed local market data, which were not available for this preliminary analysis.

## 7. Conclusions

In the study, current trends in offshore wind technology have been first critically reviewed, demonstrating that a new generation of floating wind turbines featuring LSP values, in order to better convert moderate wind speeds, can potentially disclose new sea basins and provide an increase in wind power generation needed to meet renewable energy targets. The same review showed, however, that the analyses presented to date failed in reliably estimating the potential of this technology because they made use of simplified models, which either focus on turbine components disregarding the influence of wake losses and inter-array cable layouts, or consider these effects but model the cost of turbine components using simplified cost scaling laws, which often do not include all the relevant physics. This, in turn, has led to significantly biased estimates, since changing the specific power of a FOWT has a number of implications that must be modelled.

On these bases, a new methodology for preliminarily designing LSP floating wind turbines has been developed and presented. The methodology's underlying assumptions are based on a synthesis of the best data available from academia and industry, which were reviewed and examined in the study. Once developed, the methodology, which also includes a wind farm optimization tool, has been used to assess the impact of LSP FOWTs in four case studies in the Mediterranean Sea, which – thanks to their variable characteristics in terms of wind distributions – are thought to be representative of a large number of potential moderate-wind installations worldwide.

The main takeaways of the study can be summarized as follows.

- LSP wind turbines are clearly shown to offer a promising solution in unconventional sea basins with moderate average wind speeds, both from an environmental and economic perspective. However, the optimal specific power is highly dependent on the wind resource characteristics of each site. Therefore, a comprehensive approach like the one presented here, which can go beyond the simple rotor, is mandatory to get reliable estimations.
- The lower the average wind speed, the greater the benefit due to the LSP. Among the selected study cases, a decrease in specific power has shown to lower LCoE for Sicily, Sardinia and Cyprus. For these cases, the optimal specific power ranges from 261 W/m$^2$ for Sicily (similar to a Class II site) to 175 W/m$^2$ for Cyprus, where the Weibull distribution approaches Class 4 conditions.
- Wind turbines with higher swept areas might be suboptimal in installation sites with higher average wind speeds. Although the reduced specific power results in enhanced energy production, the improvement does not compensate for the CAPEX increase, leading to higher LCoE, such as in the French site analyzed, where the reference 240 m rotor represents the most cost-effective solution.
- Wind turbines with larger swept areas also offer a reduced environmental impact compared to conventional designs. The benefits related to the increased energy output exceed the higher steel consumption, potentially lowering the overall ecological footprint. This holds true also in the cases of high wind speeds (such as the one in France discussed before), where no LCoE improvements are obtained.
- While uncertainties in component costs, such as those related to inter-array pipelines, can influence the LCoE and optimal layout, they do not necessairily affect the identification of the optimal turbine for a specific site.
- Comprehensive simulation models, such as the one developed for this study, are mandatory for critical analysis of FOWT technology, and are thought to provide in the future support to policymakers, stakeholders, and researchers for fostering the development of offshore wind in new sea basins.

## CRediT authorship contribution statement

**Riccardo Travaglini:** Methodology, Investigation, Data curation, Formal analysis, Writing – original draft. **Francesco Papi:** Conceptualization, Methodology, Supervision, Writing – review & editing. **Alessandro Bianchini:** Conceptualization, Supervision, Writing – review & editing, Project administration, Funding acquisition.

## Data availability

The aerodynamic performance map of the turbines employed in this study and the Python code used to generate the thrust and power curves are available at: DOI https://doi.org/10.5281/zenodo.14981730.

## Funding

This work has received the support of the FLOATFARM Project, funded by the European Union's H2020 research and innovation programme under grant agreement No. 101136091. Views and opinions expressed are however those of the author(s) only and do not necessarily reflect those of the European Union or the European Climate, Infrastructure and Environment Executive Agency (CINEA), which cannot be held responsible for them.

## Declaration of competing interest

The authors declare the following financial interests/personal relationships which may be considered as potential competing interests: Prof. Bianchini is currently Associated Editor of "Renewable and Sustainable Energy Reviews". He commits himself not to be involved in any way in the review process.

## Appendix A

In this Appendix, the Weibull distributions and wind roses for each installation site are presented, as well as the tables with the bathymetry and coordinates, in order to completely define the case studies. In the paragraphs below, the wind sources are described, and references are provided.

*Sicily*

**Table B.1**
Data for the installation site in Sicily.

| Site | Longitude [°] | Latitude [°] | k [t] | Median WS [m/s] | Sea depth [m] | Export distance [km] |
|---|---|---|---|---|---|---|
| Sicily [75] | 11.6371 | 37.7558 | 1.89 | 7.4 | 390 | 60 |

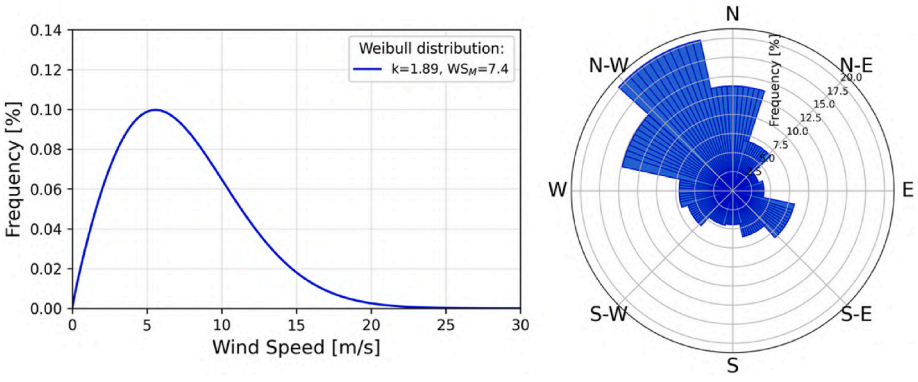


**Fig. B.1.** Weibull curve (a) and rose plot (b) of the wind source at 100 m asl for the installation site in Sicily.

*Sardinia*

**Table B.2**
Data for the installation site in Sardinia.

| Site | Longitude [°] | Latitude [°] | k [t] | Median WS [m/s] | Sea depth [m] | Export distance [km] |
|---|---|---|---|---|---|---|
| Sardinia [47] | 8.069 | 37.7558 | 1.72 | 6.4 | 300 | 35 |

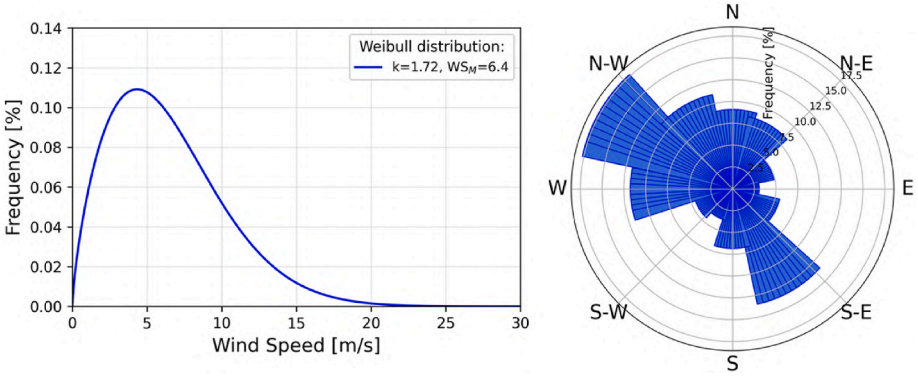


**Fig. B.2.** Weibull curve (a) and rose plot (b) of the wind source for the installation site in Sardinia.

*Cyprus*

**Table B.3**
Data for the installation site in Cyprus.

| Site | Longitude [°] | Latitude [°] | k [t] | Median WS [m/s] | Sea depth [m] | Export distance [km] |
|---|---|---|---|---|---|---|
| Cyprus [129] | 33.531647 | 34.66597 | 1.89 | 5.94 | 350 | 25 |

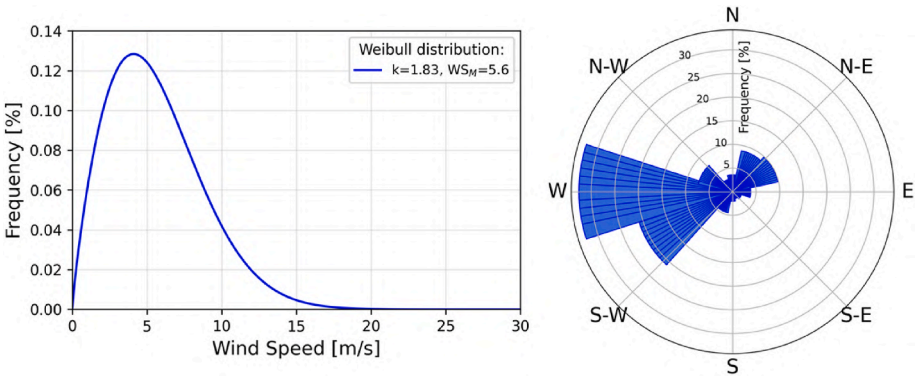


**Fig. B.3.** Weibull curve (a) and rose plot (b) of the wind source for the installation site in Cyprus.

*Lyon*

**Table B.4**
Data for the installation site in Lyon.

| Site | Longitude [°] | Latitude [°] | k [t] | Median WS [m/s] | Sea depth [m] | Export distance [km] |
|---|---|---|---|---|---|---|
| Lyon [74] | 3.397522 | 42.841737 | 1.79 | 7.6 | 85 | 20 |

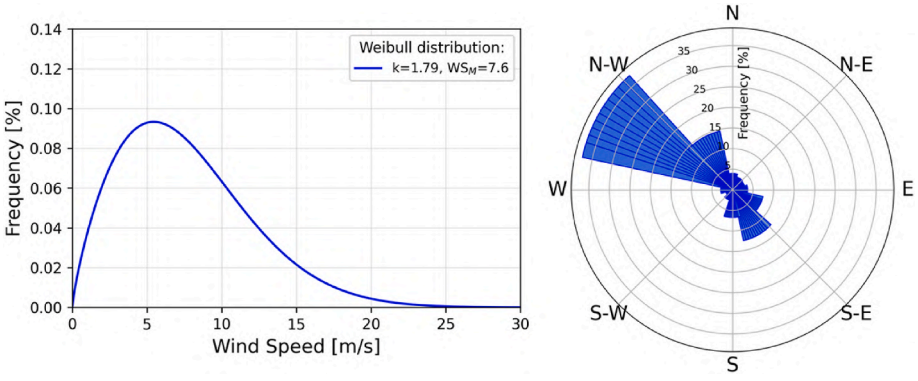


**Fig. B.4.** Weibull curve (a) and rose plot (b) of the wind source for the installation site in Lyon.

## Appendix B

In this Appendix, the cost and mass data for the semi-sub floating platforms found in the literature are presented, as well as the data relative to the tower length and weight, in order to completely define the academic and industrial state of the art.

| Rotor diameter | WT power [MW] | Steel mass [kg] | Platform cost [€] | Tower height [m] | Tower Mass [kg] | Source |
|---|---|---|---|---|---|---|
| 125 | 5 | 3.85E+06 | – | 8.76E+01 | 2.50E+05 | [130] |
| 154 | 6 | 2.30E+06 | – | 9.80E+01 | 6.70E+05 | [26] |
| 178.3 | 10 | 6.58E+06 | – | 1.07E+02 | 8.79E+05 | [82] |
| 178.3 | 10 | – | – | 1.07E+02 | 1.26E+06 | [82] |
| 216.9 | 12 | – | – | 1.10E+02 | 1.16E+06 | [90] |
| 240 | 15 | 3.91E+06 | – | 1.35E+02 | 1.26E+06 | [77] |
| 240 | 15 | – | – | 1.35E+02 | 1.09E+06 | [83] |
| 198 | 10 | 2.00E+06 | 1.38E+07 | 1.49E+02 | 7.80E+05 | [131] |
| 198 | 10 | 4.50E+06 | 3.12E+07 | 1.16E+02 | 7.80E+05 | [131] |
| 240 | 15 | 4.00E+06 | – | 1.16E+02 | 1.26E+06 | [132] |
| 240 | 15 | 4.72E+06 | – | 1.35E+02 | 1.26E+06 | [132] |
| 178.2 | 10 | 5.25E+06 | – | 1.35E+02 | 7.80E+05 | [88] |
| 198 | 10 | 4.14E+06 | – | 103.7 | 7.80E+05 | [88] |
| – | 10 | 6.37E+06 | – | 1.16E+02 | 7.80E+05 | [88] |
| 218 | 15 | 4.36E+06 | – | 1.24E+02 | 1.26E+06 | [88] |

(*continued on next page*)

(*continued*)

| Rotor diameter | WT power [MW] | Steel mass [kg] | Platform cost [€] | Tower height [m] | Tower Mass [kg] | Source |
|---|---|---|---|---|---|---|
| 240 | 15 | 4.45E+06 | – | 1.45E+02 | 1.26E+06 | [88] |
| – | 15 | 4.01E+06 | – | – | 1.26E+06 | [88] |
| – | 15 | 2.80E+06 | – | – | 1.48E+06 | [133] |
| 198 | 10 | – | 7.88E+06 | 1.16E+02 | 7.80E+05 | [134] |
| 126 | 5 | 3.59E+06 | 9.25E+06 | 8.76E+01 | 2.50E+05 | [89,135] |
| 178 | 10 | 5.60E+06 | – | 1.19E+02 | 7.04E+05 | [89] |
| 218 | 15 | 7.30E+06 | – | 1.39E+02 | 1.29E+06 | [89] |
| 252 | 20 | 8.86E+06 | – | 1.56E+02 | 2.00E+06 | [89] |
| – | 15 | 3.50E+06 | – | – | 1.48E+06 | [89] |
| 276 | 20 | 4.70E+06 | – | 1.68E+02 | 2.25E+06 | [89] |
| 310 | 25 | 6.00E+06 | – | 1.85E+02 | 3.19E+06 | [89] |
| 340 | 30 | 7.30E+06 | – | 2.00E+02 | 4.20E+06 | [89] |
| 126 | 5 | 2.50E+06 | 7.50E+06 | 1.16E+02 | 3.50E+05 | [136] |
| 125 | 5 | 3.22E+06 | 9.63E+06 | 9.00E+01 | 2.50E+05 | [58] |
| 178.3 | 10 | 4.33E+06 | 1.28E+07 | 8.76E+01 | 6.05E+05 | [58] |
| – | 15 | – | 9.00E+06 | 1.07E+02 | – | [137] |
| 125 | 5 | 3.57E+06 | – | 1.35E+02 | 6.00E+05 | [138] |
| 178.3 | 10 | 7.60E+06 | – | 8.76E+01 | 1.20E+06 | [138] |
| 125 | 5 | 3.85E+06 | – | 1.07E+02 | 2.50E+05 | [139] |
| 154 | 7.5 | 4.66E+06 | – | 7.70E+01 | 3.76E+05 | [139] |
| 154 | 7.5 | 4.55E+06 | – | 9.00E+01 | 3.76E+05 | [139] |
| 178 | 10 | 5.80E+06 | – | 9.00E+01 | 5.21E+05 | [139] |
| 178 | 10 | 5.58E+06 | – | 1.02E+02 | 5.21E+05 | [139] |
| 125 | 5 | 4.02E+06 | 6.50E+06 | 1.02E+02 | 8.82E+05 | [140] |
| 178 | 10 | 5.18E+06 | 1.00E+07 | 7.70E+01 | 1.78E+05 | [140] |
| 198 | 10 | – | 6.90E+06 | 1.07E+02 | – | [47] |
| 240 | 15 | – | 1.04E+07 | 1.16E+02 | – | [47] |
| – | 5 | – | 3.50E+06 | 1.35E+02 | – | [141] |
| – | 7 | – | 5.81E+06 | – | – | [142] |
| – | 9.5 | 3.00E+06 | – | – | – | [27] |
| – | 6 | 3.00E+06 | – | – | – | [143] |

## Data availability

Data will be made available on request.

## References


[1] European Council. European green deal. Consilium 2021. https://www.consilium.europa.eu/en/policies/green-deal/. [Accessed 5 November 2024].

[2] Desalegn B, Gebeyehu D, Tamrat B, Tadiwose T, Lata A. Onshore versus offshore wind power trends and recent study practices in modeling of wind turbines' life-cycle impact assessments. Clean Eng Technol 2023;17:100691. https://doi.org/10.1016/j.clet.2023.100691.

[3] GWEC. Global offshore wind report 2024 - global wind energy council. GLOBAL WIND ENERGY COUNCIL; 2025.

[4] Hasager CB, Hahmann AN, Ahsbahs T, Karagali I, Sile T, Badger M, et al. Europe's offshore winds assessed with synthetic aperture radar, ASCAT and WRF. Wind Energy Sci 2020;5:375–90. https://doi.org/10.5194/wes-5-375-2020.

[5] North sea programme 2022-2027. Noordzeeloket UK n.d. https://www.noordzeeloket.nl/en/policy/north-sea-programme-2022-2027/. [Accessed 5 February 2025].

[6] RVO. Dutch offshore wind market report 2023. Netherlands Enterprise Agency; 2024.

[7] RVO. Dutch Off shore Wind Innovation Guide. Your guide to Dutch offshore wind policy, technologies and innovations. Issue 2025. 2024.

[8] Correia Martins FA, Van Zuijlen A, Ferreira CS. Proof of concept for multirotor systems with vortex-generating modes for regenerative wind energy: a study based on numerical simulations and experimental data. Wind Energ Sci 2025;10:41–58. https://doi.org/10.5194/wes-10-41-2025.

[9] Stevens RJAM, Gayme DF, Meneveau C. Effects of turbine spacing on the power output of extended wind-farms. Wind Energy 2016;19:359–70. https://doi.org/10.1002/we.1835.

[10] Barthelmie RJ, Hansen K, Frandsen ST, Rathmann O, Schepers JG, Schlez W, et al. Modelling and measuring flow and wind turbine wakes in large wind farms offshore. Wind Energy 2009;12:431–44. https://doi.org/10.1002/we.348.

[11] Barthelmie RJ, Pryor SC, Frandsen ST, Hansen K, Schepers JG, Rados K, et al. Quantifying the impact of wind turbine wakes on power output at offshore wind farms. J Atmos Ocean Technol 2010;27:1302–17. https://doi.org/10.1175/2010JTECHA1398.1.

[12] Li Y, Yu W, Sciacchitano A, Ferreira C. Numerical investigation of regenerative wind farms featuring enhanced vertical energy entrainment. Wind Energy Sci Discuss 2024:1–38. https://doi.org/10.5194/wes-2024-124.

[13] Dupont E, Koppelaar R, Jeanmart H. Global available wind energy with physical and energy return on investment constraints. Appl Energy 2018;209:322–38. https://doi.org/10.1016/j.apenergy.2017.09.085.

[14] Calaf M, Meneveau C, Meyers J. Large eddy simulation study of fully developed wind-turbine array boundary layers. Phys Fluids 2010;22:015110. https://doi.org/10.1063/1.3291077.

[15] Baas P, Verzijlbergh R. The impact of wakes from neighboring wind farms on the production of the IJmuiden ver wind farm zone - whiffle. 2022.

[16] Christiansen N. Regional impacts of offshore wind farms on the north Sea hydrodynamics. Staats- und Universitätsbibliothek Hamburg Carl von Ossietzky; 2022. doctoralThesis.

[17] Pettas V, Kretschmer M, Clifton A, Cheng PW. On the effects of inter-farm interactions at the offshore wind farm Alpha Ventus. Wind Energy Sci 2021;6:1455–72. https://doi.org/10.5194/wes-6-1455-2021.

[18] Lack of grid capacity lets output of Germany's North Sea offshore wind turbines drop in 2023. Clean Energy Wire 2024. https://www.cleanenergywire.org/news/lack-grid-capacity-lets-output-germanys-north-sea-offshore-wind-turbines-drop-2023. [Accessed 19 May 2025].

[19] Glaum P, Neumann F, Brown T. Offshore power and hydrogen networks for Europe's North Sea. Appl Energy 2024;369:123530. https://doi.org/10.1016/j.apenergy.2024.123530.

[20] Gea-Bermúdez J, Das K, Pade L-L, Koivisto M, Kanellas P. NSON-DK Day-Ahead market operation analysis in the North Sea region towards 2050. Technical University of Denmark; 2019.

[21] Koivisto M, Gea-Bermúdez J, Kanellas P, Das K, Sørensen P. North Sea region energy system towards 2050: integrated offshore grid and sector coupling drive offshore wind power installations. Wind Energy Sci 2020;5:1705–12. https://doi.org/10.5194/wes-5-1705-2020.

[22] Swisher P, Murcia Leon JP, Gea-Bermúdez J, Koivisto M, Madsen HA, Münster M. Competitiveness of a low specific power, low cut-out wind speed wind turbine in North and Central Europe towards 2050. Appl Energy 2022;306:118043. https://doi.org/10.1016/j.apenergy.2021.118043.

[23] Widuto A. EU Strategy for Offshore renewable energy sources | Legislative Train Schedule. European Parliament; n.d.

[24] Zountouridou EI, Kiokes GC, Chakalis S, Georgilakis PS, Hatziargyriou ND. Offshore floating wind parks in the deep waters of Mediterranean Sea. Renew Sustain Energy Rev 2015;51:433–48. https://doi.org/10.1016/j.rser.2015.06.027.

[25] Stehly T, Duffy P. 2020 cost of wind energy review. https://doi.org/10.2172/1838135; 2021.

[26] Equinor. HYWINDSCOTLAND the world's first commercial floating wind farm. 2022.

[27] Projects: kincardine offshore wind farm - principle power, Inc. n.d. https://www.principlepower.com/projects/kincardine-offshore-wind-farm (accessed September 27, 2024).

[28] Lucas TR, Ferreira AF, Santos Pereira RB, Alves M. Hydrogen production from the WindFloat Atlantic offshore wind farm: a techno-economic analysis. Appl Energy 2022;310:118481. https://doi.org/10.1016/j.apenergy.2021.118481.
[29] Otter A, Murphy J, Pakrashi V, Robertson A, Desmond C. A review of modelling techniques for floating offshore wind turbines. Wind Energy 2022;25:831–57. https://doi.org/10.1002/we.2701.
[30] IRENA. FUTURE OF WIND. Deployment, investment, technology, grid integration and socio-economic aspects. 2019.
[31] Santhakumar S, Heuberger-Austin C, Meerman H, Faaij A. Technological learning potential of offshore wind technology and underlying cost drivers. Sustain Energy Technol Assess 2023;60:103545. https://doi.org/10.1016/j.seta.2023.103545.
[32] Bento N, Fontes M. Emergence of floating offshore wind energy: technology and industry. Renew Sustain Energy Rev 2019;99:66–82. https://doi.org/10.1016/j.rser.2018.09.035.
[33] Shields M, Beiter P, Nunemaker J. A systematic framework for projecting the future cost of offshore wind energy. Golden, CO (United States): National Renewable Energy Laboratory (NREL); 2022. https://doi.org/10.2172/1902302.
[34] DNV. Floating Offshore Wind. The next five years. 2024.
[35] Pao LY, Pusch M, Zalkind DS. Control Co-Design of wind turbines. Annu Rev Control Robot Auton Syst 2024;7:201–26. https://doi.org/10.1146/annurev-control-061423-101708.
[36] Abbas NJ, Jasa J, Zalkind DS, Wright A, Pao L. Control co-design of a floating offshore wind turbine. Appl Energy 2024;353:122036. https://doi.org/10.1016/j.apenergy.2023.122036.
[37] Mehta M, Zaaijer M, von Terzi D. Drivers for optimum sizing of wind turbines for offshore wind farms. Wind Energy Sci 2024;9:141–63. https://doi.org/10.5194/wes-9-141-2024.
[38] Serafeim G, Manolas D, Riziotis V, Chaviaropoulos P. Multidisciplinary aeroelastic optimization of a 10MW-scale wind turbine rotor targeting to reduced LCoE. J Phys Conf Ser 2022;2265:042051. https://doi.org/10.1088/1742-6596/2265/4/042051.
[39] Zalkind DS, Ananda GK, Chetan M, Martin DP, Bay CJ, Johnson KE, et al. System-level design studies for large rotors. Wind Energy Sci 2019;4:595–618. https://doi.org/10.5194/wes-4-595-2019.
[40] Buck JA, Garvey SD. Redefining the design objectives of large offshore wind turbine rotors. Wind Energy 2015;18:835–50. https://doi.org/10.1002/we.1733.
[41] Dykes K, Ning A, King R, Graf P, Scott G, Veers P. Sensitivity analysis of wind plant performance to key turbine design parameters: a systems engineering approach; preprint. Golden, CO (United States): National Renewable Energy Lab. (NREL); 2014. https://doi.org/10.2514/6.2014-1087.
[42] Shields M, Beiter P, Nunemaker J, Cooperman A, Duffy P. Impacts of turbine and plant upsizing on the levelized cost of energy for offshore wind. Appl Energy 2021;298:117189. https://doi.org/10.1016/j.apenergy.2021.117189.
[43] Ashuri T, Zaaijer MB, Martins JRRA, Zhang J. Multidisciplinary design optimization of large wind turbines—Technical, economic, and design challenges. Energy Convers Manag 2016;123:56–70. https://doi.org/10.1016/j.enconman.2016.06.004.
[44] Fingersh L, Hand M, Laxson A. Wind turbine design cost and scaling model. Golden, CO (United States): National Renewable Energy Lab. (NREL); 2006. https://doi.org/10.2172/897434.
[45] Sieros G, Chaviaropoulos P, Sørensen JD, Bulder BH, Jamieson P. Upscaling wind turbines: theoretical and practical aspects and their impact on the cost of energy. Wind Energy 2012;15:3–17. https://doi.org/10.1002/we.527.
[46] Canet H, Guilloré A, Bottasso CL. The eco-conscious wind turbine: design beyond purely economic metrics. Wind Energy Sci 2023;8:1029–47. https://doi.org/10.5194/wes-8-1029-2023.
[47] Travaglini R, Superchi F, Lanni F, Manzini G, Serri L, Bianchini A. Towards the development of offshore wind farms in the Mediterranean Sea: a techno-economic analysis including green hydrogen production during curtailments. IET Renew Power Gener 2024. https://doi.org/10.1049/rpg2.13135. n/a.
[48] Mahfouz MY, Lozon E, Hall M, Cheng PW. Integrated floating wind farm layout design and mooring system optimization to increase annual energy production. J Phys Conf Ser 2024;2767:062020. https://doi.org/10.1088/1742-6596/2767/6/062020.
[49] Yilmazlar K, Cacciola S, Xiolesmy Alfonso Rodriguez M, Croce A. Development of engineering cost models for integrated design optimization of onshore and offshore wind farms. J Phys Conf Ser 2022;2265:042042. https://doi.org/10.1088/1742-6596/2265/4/042042.
[50] NREL/floris. 2025.
[51] Hietanen AI, Snedker TH, Dykes K, Bayati I. A novel techno-economical layout optimization tool for floating wind farm design. Wind Energy Sci 2024;9:417–38. https://doi.org/10.5194/wes-9-417-2024.
[52] Cazzaro D, Pisinger D. Variable neighborhood search for large offshore wind farm layout optimization. Comput Oper Res 2022;138:105588. https://doi.org/10.1016/j.cor.2021.105588.
[53] Cao L, Ge M, Gao X, Du B, Li B, Huang Z, et al. Wind farm layout optimization to minimize the wake induced turbulence effect on wind turbines. Appl Energy 2022;323:119599. https://doi.org/10.1016/j.apenergy.2022.119599.
[54] Thomas JJ, Baker NF, Malisani P, Quaeghebeur E, Sanchez Perez-Moreno S, Jasa J, et al. A comparison of eight optimization methods applied to a wind farm layout optimization problem. Wind Energy Sci 2023;8:865–91. https://doi.org/10.5194/wes-8-865-2023.
[55] Lei Z, Gao S, Wang Y, Yu Y, Guo L. An adaptive replacement strategy-incorporated particle swarm optimizer for wind farm layout optimization. Energy Convers Manag 2022;269:116174. https://doi.org/10.1016/j.enconman.2022.116174.
[56] Yang Q, Li H, Li T, Zhou X. Wind farm layout optimization for levelized cost of energy minimization with combined analytical wake model and hybrid optimization strategy. Energy Convers Manag 2021;248:114778. https://doi.org/10.1016/j.enconman.2021.114778.
[57] Martinez A, Iglesias G. Multi-parameter analysis and mapping of the levelised cost of energy from floating offshore wind in the Mediterranean Sea. Energy Convers Manag 2021;243:114416. https://doi.org/10.1016/j.enconman.2021.114416.
[58] Ghigo A, Cottura L, Caradonna R, Bracco G, Mattiazzo G. Platform optimization and cost analysis in a floating offshore wind farm. J Mar Sci Eng 2020;8:835. https://doi.org/10.3390/jmse8110835.
[59] Lerch M, De-Prada-Gil M, Molins C, Benveniste G. Sensitivity analysis on the levelized cost of energy for floating offshore wind farms. Sustain Energy Technol Assess 2018;30:77–90. https://doi.org/10.1016/j.seta.2018.09.005.
[60] Lanni F, Serri L, Manzini G, Travaglini R, Superchi F, Bianchini A. Techno-economic analysis of sustainable hydrogen production from offshore wind farms: two Italian study cases. Processes 2025;13:1219. https://doi.org/10.3390/pr13041219.
[61] Jørgensen BH, Madsen PH, Giebel G, Martí I, Thomsen K. DTU international energy report 2021: perspectives on wind energy. DTU Wind Energy; 2021. https://doi.org/10.11581/DTU.00000200.
[62] IRENA. Renewable power generation costs in 2023. 2024.
[63] IEA Wind. IEA wind TCP task 37, definition of the IEA wind 15-Megawatt offshore reference wind turbine. 2020.
[64] Zahle F, Barlas A, Lønbæk K, Bortolotti P, Zalkind D, Wang L, et al. Definition of the IEA wind 22-Megawatt offshore reference wind turbine. Technical University of Denmark; 2024. https://doi.org/10.11581/DTU.00000317.
[65] Chirosca A-M, Rusu L. Characteristics of the wind and wave climate along the european seas focusing on the main maritime routes. J Mar Sci Eng 2022;10:75. https://doi.org/10.3390/jmse10010075.
[66] Developing the next generation of environmentally-friendly floating wind farms. Floatfarm n.d. https://floatfarm-project.eu/(accessed March 3, 2025).
[67] Serri L, Airoldi D, Lanni F, Naldi R, Castorrini A, Rispoli F, et al. Technical and economic challenges for floating offshore wind deployment in Italy and in the Mediterranean Sea. WIREs Energy Environ 2024;13:e533. https://doi.org/10.1002/wene.533.
[68] Elliott D, Bell KRW, Finney SJ, Adapa R, Brozio C, Yu J, et al. A comparison of AC and HVDC options for the connection of offshore wind generation in Great Britain. IEEE Trans Power Deliv 2016;31:798–809. https://doi.org/10.1109/TPWRD.2015.2453233.
[69] Hersbach H, Bell B, Berrisford P, Hirahara S, Horányi A, Muñoz-Sabater J, et al. The ERA5 global reanalysis. Q J R Meteorol Soc 2020;146:1999–2049. https://doi.org/10.1002/qj.3803.
[70] Yan BW, Li QS, Chan PW, He YC, Shu ZR. Characterising wind shear exponents in the offshore area using lidar measurements. Appl Ocean Res 2022;127:103293. https://doi.org/10.1016/j.apor.2022.103293.
[71] International Electrochemical commission. IEC 61400-1:2019 wind energy generation systems - part 1: design requirements n.d.
[72] General information Nederwiek. Offshorewind RVO 2022. https://offshorewind.rvo.nl/cms/view/91063764-5eb7-428e-9c6e-e38fcf3adf22/general-information-nederwiek. [Accessed 19 June 2024].
[73] Davis NN, Badger J, Hahmann AN, Hansen BO, Mortensen NG, Kelly M, et al. The global wind atlas: a high-resolution dataset of climatologies and associated web-based application. https://doi.org/10.1175/BAMS-D-21-0075.1; 2023.
[74] Les Éoliennes Flottantes du Golfe du Lion - principle Power, Inc. n.d. https://www.principlepower.com/projects/les-eoliennes-flottantes-du-golfe-du-lion (accessed December 5, 2024).
[75] Renexia. MED WIND an innovative floating offshore wind farm in the heart of the mediterranean. https://renexia.it/en/med-wind-projects/. [Accessed 18 November 2024].
[76] Severini L. Parco eolico flottante nel mare di Sardegna Sud coccidentale. 2020.
[77] Dagher JH, Goupee AJ, Viselli AM. Optimized floating offshore wind turbine substructure design trends for 10–30 MW turbines in Low-, Medium-, and high-severity wave environments. Designs 2024;8:72. https://doi.org/10.3390/designs8040072.
[78] User guide — TOPFARM 2.4.0.post1 documentation n.d. https://topfarm.pages.windenergy.dtu.dk/TopFarm2/user_guide.html#dtu-cost-model. [Accessed 26 November 2024].
[79] IEA-15-240-RWT/OpenFAST/IEA-15-240-RWT/Cp_Ct_Cq.IEA15MW.txt at master · IEAWindTask37/IEA-15-240-RWT. GitHub n.d. https://github.com/IEAWindTask37/IEA-15-240-RWT/blob/master/OpenFAST/IEA-15-240-RWT/Cp_Ct_Cq.IEA15MW.txt (accessed January 16, 2025).
[80] Saint-Drenan Y-M, Besseau R, Jansen M, Staffell I, Troccoli A, Dubus L, et al. A parametric model for wind turbine power curves incorporating environmental conditions. Renew Energy 2020;157:754–68. https://doi.org/10.1016/j.renene.2020.04.123.
[81] Sim S-K, Peinke J, Maass P. Signatures of geostrophic turbulence in power spectra and third-order-structure function of offshore wind speed fluctuation. https://doi.org/10.48550/arXiv.2203.07685; 2023.
[82] Lerch M. Qualification of innovative floating substructures for 10MW wind turbines and water depths greater than 50m. | LIFES 50plus project | fact sheet | H2020. CORDIS | European Commission 2019.
[83] Mahfouz MY, Salari M, Hernández S, Molins C, Trubat P, Bredmose H, et al. Public design and FAST models of the two 15MW floater-turbine concepts. USTUTT/UPC/COBRA/ESTYCO/DTU; 2020.

[84] IEA. turbine-models/Offshore/IEA_15MW_240_RWT.csv at master · NREL/turbine-models. GitHub 2020. https://github.com/NREL/turbine-models/blob/master/Offshore/IEA_15MW_240_RWT.csv. [Accessed 17 February 2024].
[85] NREL. IEAWindTask37/IEA-22-280-RWT 2024. https://github.com/IEAWindTask37/IEA-22-280-RWT. [Accessed 26 November 2024].
[86] Papi F, Bianchini A. Technical challenges in floating offshore wind turbine upscaling: a critical analysis based on the NREL 5 MW and IEA 15 MW reference turbines. Renew Sustain Energy Rev 2022;162:112489. https://doi.org/10.1016/j.rser.2022.112489.
[87] Robertson AN, Jonkman JM. Loads analysis of several offshore floating wind turbine concepts. Golden, CO (United States): National Renewable Energy Lab. (NREL); 2011.
[88] Wu J, Kim M-H. Generic upscaling methodology of a floating offshore wind turbine. Energies 2021;14:8490. https://doi.org/10.3390/en14248490.
[89] Roach KL, Lackner MA, Manwell JF. A new methodology for upscaling semi-submersible platforms for floating offshore wind turbines. Wind Energy Sci 2023;8:1873–91. https://doi.org/10.5194/wes-8-1873-2023.
[90] Sergiienko NY, da Silva LSP, Bachynski-Polić EE, Cazzolato BS, Arjomandi M, Ding B. Review of scaling laws applied to floating offshore wind turbines. Renew Sustain Energy Rev 2022;162:112477. https://doi.org/10.1016/j.rser.2022.112477.
[91] Liu Y, Zhang J-M, Min Y-T, Yu Y, Lin C, Hu Z-Z. A digital twin-based framework for simulation and monitoring analysis of floating wind turbine structures. Ocean Eng 2023;283:115009. https://doi.org/10.1016/j.oceaneng.2023.115009.
[92] Gaidai O, Yakimov V, Wang F, Zhang F, Balakrishna R. Floating wind turbines structural details fatigue life assessment. Sci Rep 2023;13:16312. https://doi.org/10.1038/s41598-023-43554-4.
[93] DNV. DNV-RP-0286 Coupled analysis of floating wind turbines. n.d.
[94] American Bureau of Shipping. Guide for building and classing, FLOATING OFFSHORE WIND TURBINE INSTALLATIONS. n.d.
[95] Zalkind D, Bortolotti P. Control Co-Design studies for a 22 MW semisubmersible floating wind turbine platform. J Phys Conf Ser 2024;2767:082020. https://doi.org/10.1088/1742-6596/2767/8/082020.
[96] Release Fix nacelle mass properties · IEAWindSystems/IEA-15-240-RWT. GitHub n.d https://github.com/IEAWindSystems/IEA-15-240-RWT/releases/tag/v1.1.11 (accessed March 5, 2025).
[97] Release v1.0.1 · IEAWindSystems/IEA-22-280-RWT. GitHub n.d. https://github.com/IEAWindSystems/IEA-22-280-RWT/releases/tag/v1.0.1 (accessed March 5, 2025).
[98] Maness M, Smith A, Maples B. NREL offshore balance-of-system model. 2017.
[99] Major D, Schmitz S. The optimum range of design axial induction factors for lowest levelized-cost of energy. Wind Energy Sci Discuss 2024:1–47. https://doi.org/10.5194/wes-2024-109.
[100] Mehta M. Turbine sizing for electricity and hydrogen production. https://doi.org/10.5281/zenodo.8380355; 2023.
[101] Welcome to TOPFARM — TOPFARM 2.3.4 documentation n.d. https://topfarm.pages.windenergy.dtu.dk/TopFarm2/index.html. [Accessed 19 June 2024].
[102] Welcome to PyWake — PyWake 2.6.3. dev3+gd6ee25a documentation n.d. https://topfarm.pages.windenergy.dtu.dk/PyWake/index.html (accessed June 19, 2024).
[103] Lundtang Petersen E, Troen I, Ejsing Jørgensen H, Mann J. The new European wind atlas. Energy Bull 2014:34–9.
[104] IEC TS 61400-3-2:2019 | IEC webstore n.d. https://webstore.iec.ch/publication/29244 (accessed January 3, 2023).
[105] Bastankhah M, Porté-Agel F. A new analytical model for wind-turbine wakes. Renew Energy 2014;70:116–23. https://doi.org/10.1016/j.renene.2014.01.002.
[106] Porté-Agel F, Bastankhah M, Shamsoddin S. Wind-turbine and wind-farm flows: a review. Bound-Layer Meteorol 2020;174:1–59. https://doi.org/10.1007/s10546-019-00473-0.
[107] Katic I, Højstrup J, Jensen NO. A simple model for cluster efficiency: european wind energy association conference and exhibition. EWEC86 Proc 1987;1:407–10.
[108] Superposition models — PyWake 2.6.8.dev26+g5562afda documentation n.d. https://topfarm.pages.windenergy.dtu.dk/PyWake/notebooks/SuperpositionModels.html#LinearSum (accessed February 10, 2025).
[109] Rotor average models — PyWake documentation n.d. https://topfarm.pages.windenergy.dtu.dk/PyWake/notebooks/RotorAverageModels.html (accessed February 10, 2025).
[110] Pierik JTG, Dekker JWM, Braam H, Bulder BH, Winkelaar D, Larsen GChr, et al. European wind turbine standards II (EWTS-II): 1999 European wind energy conference and exhibition. Wind Energy Millenn Proc 1999:568–71.
[111] Réthoré P-E, Fuglsang P, Larsen TJ, Buhl T, Larsen GChr. TOPFARM wind farm optimization tool. Risø national laboratory for sustainable energy. Technical University of Denmark; 2011.
[112] TOPFARM/EDWIN · GitLab. GitLab 2024. https://gitlab.windenergy.dtu.dk/TOPFARM/edwin. [Accessed 6 February 2025].
[113] Alencar MS de. Mdealencar/Interarray. 2025.
[114] OpenMDAO. GitHub n.d. https://github.com/OpenMDAO (accessed December 4, 2024).
[115] Kheirabadi AC, Nagamune R. Real-time relocation of floating offshore wind turbine platforms for wind farm efficiency maximization: an assessment of feasibility and steady-state potential. Ocean Eng 2020;208:107445. https://doi.org/10.1016/j.oceaneng.2020.107445.
[116] Froese G, Ku SY, Kheirabadi AC, Nagamune R. Optimal layout design of floating offshore wind farms. Renew Energy 2022;190:94–102. https://doi.org/10.1016/j.renene.2022.03.104.
[117] Rodrigues SF, Teixeira Pinto R, Soleimanzadeh M, Bosman PAN, Bauer P. Wake losses optimization of offshore wind farms with moveable floating wind turbines. Energy Convers Manag 2015;89:933–41. https://doi.org/10.1016/j.enconman.2014.11.005.
[118] B.3 Mooring system | Guide to a floating offshore wind farm. n.d.
[119] Allen C, Viscelli A, Dagher H, Goupee A, Gaertner E, Abbas N, et al. Definition of the UMaine VolturnUS-S reference platform developed for the IEA wind 15-Megawatt offshore reference wind turbine. Golden, CO (United States); Univ. of Maine, Orono, ME (United States): National Renewable Energy Lab. (NREL); 2020. https://doi.org/10.2172/1660012.
[120] ESG. Esg - ecology weighs Most heavily in offshore wind tenders. ABN AMRO Bank; 2024. https://www.abnamro.com/research/en/our-research/esg-economist-ecology-weighs-most-heavily-in-offshore-wind-tenders (accessed March 6, 2025).
[121] ERM. Offshore wind tenders: how developers can gain the edge with circularity. Electro Retail Mag (ERM) 2024. https://www.erm.com/insights/offshore-wind-tenders-how-developers-can-gain-the-edge-with-circularity/ (accessed March 6, 2025).
[122] What is the carbon footprint of steel? Sustain Ships n.d. https://www.sustainable-ships.org/stories/2022/carbon-footprint-steel (accessed March 4, 2025).
[123] CO2 emissions per kWh in Italy - nowtricity n.d. https://www.nowtricity.com/country/italy/. [Accessed 21 January 2025].
[124] CO2 emissions per kWh in France - nowtricity n.d. https://www.nowtricity.com/country/france/. [Accessed 22 January 2025].
[125] Nowtricity n.d. https://www.nowtricity.com/. [Accessed 19 February 2025].
[126] Ribnitzky D, Berger F, Petrović V, Kühn M. Hybrid-lambda: a low-specific-rating rotor concept for offshore wind turbines. Wind Energy Sci 2024;9:359–83. https://doi.org/10.5194/wes-9-359-2024.
[127] Simpson J, Loth E, Dykes K. Cost of valued energy for design of renewable energy systems. Renew Energy 2020;153:290–300. https://doi.org/10.1016/j.renene.2020.01.131.
[128] Superchi F, Mustakis A, Pechlivanoglou G, Bianchini A. Application of the cost of valued energy (COVE) to a RES-Based hybrid energy system on a mediterranean island to evaluate the potential of energy storage systems. IET Conf Proc 2023;2023:178–85. https://doi.org/10.1049/icp.2023.1568.
[129] Προκοπίου Ε. Εδώ προορίζονται τα πλωτά αιολικά πάρκα στην Κύπρο – Χάρτης. Philenews 2025. https://www.philenews.com/oikonomia/kypros/article/1545866/edo-proorizonte-ta-plota-eolika-parka-stin-kipro-chartis/. [Accessed 4 March 2025].
[130] Robertson A, Jonkman J, Masciola M. Definition of the semisubmersible floating system for phase II of OC4. Golden, CO (United States): National Renewable Energy Lab. (NREL); 2014.
[131] Oh S. Comparison of concrete and steel semisubmersible floaters for 10MW wind turbines. ClassNK 2021.
[132] Ivanov G, Hsu I-J, Ma K-T. Design considerations on semi-submersible columns, bracings and pontoons for floating wind. J Mar Sci Eng 2023;11:1663. https://doi.org/10.3390/jmse11091663.
[133] Sener. HiveWind - semi-submersible floating steel platform for offshore wind turbines. Sener 2021.
[134] Ferri G, Marino E, Bruschi N, Borri C. Platform and mooring system optimization of a 10 MW semisubmersible offshore wind turbine. Renew Energy 2022;182:1152–70. https://doi.org/10.1016/j.renene.2021.10.060.
[135] Katsouris G, Marina A. Cost modelling of floating wind farms. ECN; 2016.
[136] Bjerkseter C, Agotnes A. Levelized cost of energy for offshore floating wind turbine concepts. n.d.
[137] Boscarino E. Progetto di un parco eolico offshore di tipo galleggiante della potenza complessiva di 555 MW, denominato “Calabria” da realizzarsi nello specchio acqueo del Golfo di Squillace a largo di Punta Stilo e delle relative opere di connessione alla Rete di Trasmissione Nazionale (RTN) - documentazione - valutazioni e Autorizzazioni Ambientali - VAS - VIA - AIA. STIMA PRELIMINARE DELLE OPERE E QUADRO ECONOMICO. MPOWER S.r.l.; n.d.
[138] Leimeister M, Bachynski EE, Muskulus M, Thomas P. Rational upscaling of a semi-submersible floating platform supporting a wind turbine. Energy Proc 2016;94:434–42. https://doi.org/10.1016/j.egypro.2016.09.212.
[139] George j. WindFloat design for different turbine sizes. Lisboa: Instituto Superior Técnico; 2014.
[140] Kikuchi Y, Ishihara T. Upscaling and levelized cost of energy for offshore wind turbines supported by semi-submersible floating platforms. J Phys Conf Ser 2019;1356:012033. https://doi.org/10.1088/1742-6596/1356/1/012033.
[141] Castro-Santos L, Diaz-Casas V. Economic influence of location in floating offshore wind farms. Ocean Eng 2015;107:13–22. https://doi.org/10.1016/j.oceaneng.2015.07.025.
[142] Heidari S. Economic modelling of floating offshore wind power : calculation of levelized cost of energy. 2017.
[143] GWEC. Global wind report 2021 - global wind energy council. GLOBAL WIND ENERGY COUNCIL; 2021.